

3-23-2017

Modeling the White Sands Missile Range Fast Burst Reactor Using a Discrete Ordinates Code, PENTRAN

Taylor R. Schulmeister

Follow this and additional works at: <https://scholar.afit.edu/etd>

Part of the [Nuclear Commons](#)

Recommended Citation

Schulmeister, Taylor R., "Modeling the White Sands Missile Range Fast Burst Reactor Using a Discrete Ordinates Code, PENTRAN" (2017). *Theses and Dissertations*. 1625.
<https://scholar.afit.edu/etd/1625>

This Thesis is brought to you for free and open access by the Student Graduate Works at AFIT Scholar. It has been accepted for inclusion in Theses and Dissertations by an authorized administrator of AFIT Scholar. For more information, please contact richard.mansfield@afit.edu.



**MODELING THE WHITE SANDS MISSILE RANGE FAST BURST REACTOR
USING A DISCRETE ORDINATES CODE, PENTRAN**

THESIS

Taylor R. Schulmeister, 1st Lieutenant, USAF

AFIT-ENP-MS-17-M-104

**DEPARTMENT OF THE AIR FORCE
AIR UNIVERSITY**

AIR FORCE INSTITUTE OF TECHNOLOGY

Wright-Patterson Air Force Base, Ohio

**DISTRIBUTION STATEMENT A.
APPROVED FOR PUBLIC RELEASE; DISTRIBUTION UNLIMITED.**

The views expressed in this thesis are those of the author and do not reflect the official policy or position of the United States Air Force, Department of Defense, or the United States Government. This material is declared a work of the U.S. Government and is not subject to copyright protection in the United States.

AFIT-ENP-MS-17-M-104

MODELING THE WHITE SANDS MISSILE RANGE FAST BURST REACTOR
USING A DISCRETE ORDINATES CODE, PENTRAN

THESIS

Presented to the Faculty

Department of Engineering Physics

Graduate School of Engineering and Management

Air Force Institute of Technology

Air University

Air Education and Training Command

In Partial Fulfillment of the Requirements for the

Degree of Master of Science

Taylor R. Schulmeister, BS

1st Lieutenant, USAF

March 2017

DISTRIBUTION STATEMENT A.
APPROVED FOR PUBLIC RELEASE; DISTRIBUTION UNLIMITED.

AFIT-ENP-MS-17-M-104

MODELING THE WHITE SANDS MISSILE RANGE FAST BURST REACTOR
USING A DISCRETE ORDINATES CODE, PENTRAN

Taylor R. Schulmeister, BS

1st Lieutenant, USAF

Committee Membership:

Lt Col J. R. Fee, PhD
Chair

Lt Col B. J. Singleton, PhD
Member

Dr. G. E. Sjoden, PhD
Member

Abstract

The goal of this research was to develop and characterize a deterministic model of a fast burst reactor (FBR) using a discrete ordinates neutral particle transport code, PENTRAN. The White Sands Missile Range FBR design was chosen for this research because of its strategic importance to the DoD. Specifically, it produces a very short duration, high energy neutron flux which is representative of the neutron flux output created by a nuclear weapon. One, two, and three dimensional PENTRAN models of the FBR were developed and neutron transport based eigenvalue calculations were performed. These eigenvalue calculations were conducted using two different sets of nuclear cross-section data: the Bugle-96 47-energy group library (intended for a thermal reactor design), and a collapsed 10-group version of the Bugle-96 library which captured the fast neutron energy groups and a single thermal group. The PENTRAN neutron transport calculation results were compared to an analogous MCNP Monte Carlo model using continuous energy neutron cross sections. The least computationally expensive PENTRAN neutron flux calculations, which also compares favorably with the MCNP calculations, was a 24 direction S4 P_n - T_n based quadrature with a first order Legendre Polynomial (P1) expansion of the scattering term and the 10 energy group neutron cross-section library. Future work is required to refine the model because the modeled configuration results in a supercritical system when such a configuration should produce a subcritical system.

Acknowledgments

I would like to thank my fellow 17M ENP classmates who made my AFIT experience enjoyable.

Taylor R. Schulmeister

Table of Contents

	Page
Abstract	iv
Table of Contents	vi
List of Figures	viii
List of Tables	ix
I. Introduction	1
General Issue	1
Problem Statement.....	3
Research Focus.....	3
Methodology.....	3
Assumptions	4
Implications	6
II. Literature Review	7
Chapter Overview.....	7
Fast Burst Reactors in the U.S.A. [4]	7
Optimization of Multi-Group Cross Sections for Fast Reactor Analysis [3]	10
PENTRAN User's Guide Version 9.4X.7 [2]	11
PENMSHXP Manual [7].....	12
Neutral Particle Transport Theory.....	14
The Boltzmann Transport Equation	16
Parallel Processing Theory	18
Summary.....	19
III. Methodology	21
Chapter Overview.....	21

FBR Model Construction	21
Summary.....	39
IV. Analysis and Results.....	40
Chapter Overview.....	40
Simulation Results.....	40
Leakage Analysis.....	49
Flux Scaling Factors	51
Model Refinement	51
Summary.....	54
V. Conclusions and Recommendations	55
Significance of Research	56
Recommendations for Future Research.....	57
Appendix A. PENMSHXP/PENTRAN Input Files.....	59
Bibliography	99

List of Figures

	Page
Figure 1. WSMR FBR Diagram	8
Figure 2. 1D FBR Model	21
Figure 3. PENTRAN Coarse Mesh Example	24
Figure 4. Multiple Coarse Mesh Example	26
Figure 5. Non-Critical FBR Mesh	29
Figure 6. WSMR FBR Z-Level 1	32
Figure 7. WSMR FBR Z-Level 2	33
Figure 8. WSMR FBR Z-Level 3	34
Figure 9. WSMR FBR Z-Level 4	35
Figure 10. WSMR FBR Z-Level 5	36
Figure 11. WSMR FBR Z-Level 6	37
Figure 12. PENTRAN Flux Plot S8 P0 47G 1.3534-1.653 MeV	43
Figure 13. PENTRAN Flux Plot S4 P0 47G 1.3534-1.653 MeV	44
Figure 14. WSMR FBR MCNP Model.....	46
Figure 15. Air Flow Grooves Z-level 2	52
Figure 16. Air Flow Grooves Z-Level 3	53

List of Tables

	Page
Table 1. Color Legend for WSMR Model Materials	25
Table 2. Dimensions for WSMR FBR PENTRAN Model	28
Table 3. Z-Level Dimensions for WSMR FBR Model.....	31
Table 4. Energy Groups of Bugle-96 Library	40
Table 5. Energy Groups of Collapsed 10 Group Library.....	42
Table 6. Criticalities of PENTRAN/MCNP Runs	45
Table 7. Material Balance Information	48
Table 8. Neutron Leakage Location Information	50
Table 9. Flux Scaling Factors	51

MODELING THE WHITE SANDS MISSILE RANGE FAST BURST REACTOR USING A DISCRETE ORDINATES CODE, PENTRAN

I. Introduction

General Issue

The White Sands Missile Range (WSMR) Fast Burst Reactor (FBR) is the most widely used fast burst reactor for Department of Defense (DoD) research into the effects that nuclear weapon radiation will have on electronic components and systems. [1] The FBR is expensive to operate and any single experiment has a limited time to utilize the FBR output. Therefore, it is critical that the reactor neutron flux characteristics are understood prior to conducting an experiment. To aid this understanding, modeling and simulation tools have been used extensively for design of experiment purposes. The most prominent transport code used for this purpose is the Monte Carlo N-Particle Transport Code (MCNP). While the Monte Carlo method is the “gold standard” in industry for transport computations, this method of solving the neutron transport equation has several distinct disadvantages, which makes the exploration of a different solution approach a worthwhile endeavor. Among these disadvantages, MCNP was not designed from the ground up to execute calculations in a parallel fashion. While the code is capable of tasking multiple processors, it is not uncommon for complex problems to take hours or days to solve. Additionally, when MCNP solves a transport problem, it does so by calculating the statistical average flux through a surface at specific tally points, as opposed to providing flux values at all points on the model.

PENTRAN (Parallel Environment Neutral-Particle TRANsport) is a deterministic code that can be used as an alternative to the Monte Carlo method for radiation transport that was designed to be highly parallelizable. This capability allows for complex multiple neutron energy group geometric problems to be analyzed in a matter of minutes, with significant time reductions being realized as the number of processors is increased. Furthermore, because PENTRAN solves the complete phase space of the transport problem deterministically, it explicitly computes the flux at any point on a surface, yielding a significant advantage to MCNP when such calculations become important to the problem at hand. [2] PENTRAN achieves this because it is a discrete ordinates code, meaning that instead of using a continuum of angles and energies stochastically sampled using distribution functions as MCNP does, the user must specify the allowed spatial mesh, and discrete energies and angles. Specifying the discretized quantities allows for processor decomposition based on energy, angle, and space, significantly increasing the efficiency of flux calculations. PENTRAN has been validated and verified to be capable of accurately modeling a myriad of thermal reactor designs in addition to fast breeder reactor designs. If PENTRAN can be verified as an accurate model for fast burst reactors as well, the design of experiment applications for the DoD at the WSMR FBR facility are nearly limitless. [2]

Problem Statement

PENTRAN has been verified and validated with models of both thermal and fast breeder nuclear reactors. This research will develop a PENTRAN model of the WSMR FBR and verify the accuracy of the model. Then, an attempt will be made to decrease the run time and memory requirements through cross-section library modification.

Research Focus

The focus of this research is to construct a PENTRAN model of the WSMR FBR in order to simulate the neutron flux output of this reactor. The PENTRAN model will then be compared to an analogous MCNP model for verification purposes.

Methodology

The 47-energy group neutron cross section library Bugle-96 will be used as the basis to form a cross section that primarily contains fast energy groups. The process of reducing the 47-energy group library to a library with less energy groups that is representative of the neutron population at the FBR will be referred to as “collapsing the energy groups”. The Bugle-96 library is designed to be used for thermal reactors but was the only library readily available for this research. However, this library should have sufficient energy groups above 0.1 MeV to capture the fast neutron energy groups needed for the FBR design. The creation of an accurate model to represent the WSMR FBR was done in three progressive research phases. The first phase created a one-dimensional model with representative dimensions and materials. This model was employed to build the new cross section library from the Bugle-96 47 group cross-section data. In addition, this model served as a proof of concept and provided insight into the 2 and 3-D models.

The second effort created a two-dimensional model of the WSMR FBR in a number of configurations (burst/control rods in or out, safety block in or out) and calculations using the collapsed library will be compared against calculations with the full 47 group library. Finally, during the third effort a three-dimensional model of the WSMR FBR was developed for an accurate representation of the reactor design. When the three-dimensional model has been developed, PENTRAN neutron flux calculations were then compared to MCNP calculations to begin to verify and validate the accuracy of the PENTRAN model for a fast burst reactor design.

A one dimensional, two dimensional, and three-dimensional model of the WSMR FBR were constructed in PENTRAN and neutron flux calculations were performed. The 47 group Bugle-96 neutron library was collapsed down to fewer energy groups using a process detailed in the open literature. [3] Comparisons of eigenvalue calculations were made between using the collapsed 10 group version of the standard 47 group Bugle-96 cross-section database. Upon successfully calculating neutron flux profiles for the WSMR FBR, these results were compared to MCNP flux calculations. With this data available a well informed decision regarding the merits of PENTRAN to model a fast burst reactor could be made.

Assumptions

As with any modeling and simulation research effort, a number of assumptions must be made to allow for representation of the real world scenario in a virtual environment confined by programming restraints. Many of the assumptions made during construction of the PENTRAN FBR models relate to dimensions of items within or

around the fuel assembly. The WSMR FBR model was based upon the 1965 paper “FAST BURST REACTORS IN THE U.S.A.” This reference was used exclusively to obtain dimensions and specifications for several FBR components. [4] These components include: the fuel assembly, safety block, support plate, Inconel bolts, and stainless-steel core. This article fails to provide dimensions for the control rods, burst rod, mass adjustment ring, and shroud. As a result, assumptions were made regarding the dimensions of these components. Additionally, due to the nature of a discrete ordinates code, only specified angles and energies were allowed when the particles scattered. This is not the case in reality, where a continuum of energies and angles exists.

Limitations to the fidelity of the model come primarily in the form of constraints to the available memory of the system the simulation is run on. The three dimensional model, with dimensions of x, y, and z, consists of multiple unique z-levels. Each z-level is divided into a series of coarse meshes. These coarse meshes are regions of the z-level which are chosen by the user in a configuration that allows for the problem to be spread across multiple processors. In the case of the FBR model 16 coarse meshes were used per z-level to allow for ideal decomposition of the problem across the processors available. Each coarse mesh is further subdivided into smaller regions by what are called fine meshes. These fine meshes add fidelity to the model at the expense of increasing the memory needed per processor. Because of this, there is a limit on the number of fine meshes, or level of detail, that can be applied, with that limit being directly related to the amount of memory available per processor.

Implications

This research should determine the viability of using PENTRAN to model a fast reactor. If PENTRAN can model fast burst reactors, specifically the FBR, then it will be possible for future researchers to use this capability for design of experiment applications for future experimentation at the FBR. Additionally, this research furthered the research agreement between the Air Force Institute of Technology (AFIT) and the Air Force Technical Application Center (AFTAC) who sponsored it. [5] Finally, PENTRAN provided a code to compare against for current MCNP FBR modeling efforts being performed by the Defense Threat Reduction Agency (DTRA) in conjunction with AFIT students and faculty. [6]

II. Literature Review

Chapter Overview

The purpose of this chapter is to identify relevant research regarding the use of PENTRAN to model fast burst reactors. Throughout this chapter, several articles and manuals will be discussed. The intent of this chapter is to identify the work that others have performed in this research area and identify how this research effort will enhance the understanding of the accuracy of PENTRAN in modeling a fast burst reactor design. Additionally, this chapter will cover the source of measurements and information on the WSMR FBR. Finally, the theory behind neutral particle transport and parallel processing, and respective uses will be highlighted. The intent of this chapter is not in depth discussion of neutron transport and parallel processing theory, but rather to provide detail upon the facets of those theories that had a direct impact on this research effort.

Fast Burst Reactors in the U.S.A. [4]

The reactor located at WSMR is called the Molly-G design. This is short for molybdenum-alloy Godiva, which is a reference to the Godiva II reactor created by Los Alamos National Laboratory (LANL) [4]. The fuel mass for the WSMR FBR is 97 kilograms (kg) and it is composed of 90 weight-percent uranium, and 10 weight-percent molybdenum. A diagram of the WSMR FBR can be seen in Figure 1.

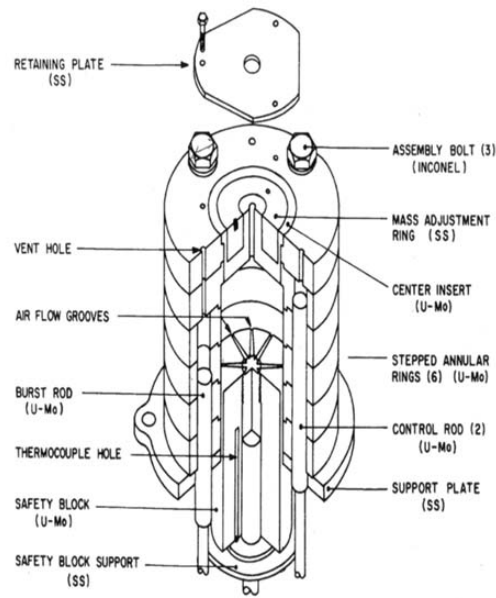


Figure 1. WSMR FBR Diagram [4]

The report “FAST BURST REACTORS IN THE U.S.A.” provides a number of dimensions for the WSMR FBR and was the foundation for building the model. When creating a reactor model, knowing the dimensions of the various reactor components is critically important because the dimensions of the reactor components greatly affect the criticality of the model. Also, the dimensions directly affect the flux at any point on the model. If a model has too much fuel, it will over-predict the criticality of the system. If the amount of simulated fuel is too low, the criticality will be under predicted leading to lower flux values.

The materials of the reactor components are identified by the report “Fast Burst Reactors in the USA.” The makeup of these materials has significant implications when performing flux calculations due to the changing nuclear cross-section data for each material at a given energy. The manufacturers of the FBR used boron’s high thermal

neutron absorption cross-section to their advantage by surrounding the fuel assembly with a boron-loaded silicate shroud. This boron loaded silicate shroud has a high probability of reacting with the thermal neutrons (several hundred keV or less) and absorbs them. While not all thermal neutrons are absorbed by the shroud, the amount that escapes is minimal. However, high energy neutrons (several keV to MeV) have a low probability of interaction with the boron loaded silicate shroud due to their nuclear cross-sections not presenting a high probability of reacting with high energy neutrons. Thus, the vast majority of the neutrons that escape the shroud are high energy neutrons, while low energy neutrons make up only a small fraction of the neutrons that enter the test chamber.

While the report “Fast Burst Reactors in the USA” proved invaluable to this research effort, it did not include dimensions for all components of the reactor. In order to determine dimensions for these unspecified components, an assumption was made that the diagram seen in Figure 1 was to scale. Subsequently, an engineering analysis was conducted on this diagram and component dimensions were obtained. In addition to being used to estimate the dimensions of components not explicitly called out in the paper, this diagram was used to conceptually place reactor components during model creation.

Optimization of Multi-Group Cross Sections for Fast Reactor Analysis [3]

The selection of nuclear cross-section data for a reactor model has an impact on the predictions of reactions that occur in the constituent materials made by the model. Because the average energy of the FBR neutron flux outputs is in the fast portion of the neutron energy spectrum, using nuclear cross-section data designed for power reactors, which have an average energy in the thermal portion, would improperly represent interaction probabilities for the reactor design. However, the Bugle-96 library, designed for power reactors, was the nuclear cross-section library which was readily available for use with this study. A study conducted by the Nuclear and Radiological Engineering Program of the Georgia Institute of Technology (GaTech) performed an optimization study to identify the ideal multi-group cross-sections when modeling a fast burst reactor design.

The research effort conducted by GaTech began with a library of nuclear cross-section data for 238 energy groups and attempted to collapse these cross sections to as few energy groups as possible while maintaining flux predictions that were representative of using all of the energy groups. The GaTech research sought to reduce the number of energy groups because the number of energy groups is directly proportional to the number of required equations to solve which means that the amount of memory per processor increases, forcing users to run the program on more processors. The GaTech research demonstrated a library of nuclear cross-section data for 10 energy groups that was representative of the original 238 energy group library. With this 10-group library, the GaTech team calculated the fast breeder criticality to within three percent of the criticality achieved using the 238-group library [3]. During this thesis research,

comparisons will be made between PENTRAN calculations performed using both the 10 and 47 group libraries.

PENTRAN User's Guide Version 9.4X.7 [2]

The PENTRAN manual details the control options that are present in a PENTRAN execution file. Within the PENTRAN execution file quadrature scheme, processor decomposition and boundary conditions can be set along with numerous other settings not relevant to this research. This manual also details commonly occurring errors and offers potential troubleshooting steps to resolve these issues.

PENTRAN execution files are broken into sections referred to as blocks. Each execution file has 7 blocks. Additionally, parameters for memory allocation are located prior to block 1. Memory allocation parameter settings are located on page 88 of the PENTRAN manual and describe a range of memory related settings such as the maximum number of energy groups to be handled in the problem, the number of processors available for usage, and the amount of memory per processor available for calculations. The first block of a PENTRAN problem contains general problem information and each block 1 parameter is described on page 99 of the PENTRAN manual. Of particular importance in this block is the decmpv setting, which controls how available processors will be allocated to perform the calculations. The processors can be allocated into solving angular calculations, energy group calculations, or spatial calculations. Block 2 contains the geometry of the problem as well as the initial flux value. Block 2 settings are detailed on pg. 106 of the PENTRAN Manual. Block 3 is where the cross section parameters are located. In this block, the file containing cross

section data is specified, the Legendre order of the cross-sections is indicated, and the file containing chi values is entered. Block 3 settings are described on pg. 108 of the PENTRAN manual. Block 4 consists of control options. These settings control things such as the number of iterations PENTRAN will perform before stopping, convergence criteria, and the differencing method used on each coarse mesh. Block 4 settings are discussed on pg. 111. Block 5 is the location of source definitions and options. Within block 5, the location and type of sources can be entered. PENTRAN can run with or without fixed sources, and for this research, no fixed sources were placed in the model. Block 5 options are noted on pg. 117. Block 6 contains settings for the boundary conditions. In this block, boundaries can be set to reflective or absorptive. Reflective boundaries allow for the inherently three dimensional PENTRAN calculations to simulate a one or two-dimensional environment. Block 6 parameters are described on pg. 121 of the PENTRAN manual. Block 7 contains print options. In this block settings can be chosen to print source distribution tables, scalar flux moments, angular flux data, and several other data items. The settings for printing parameters can be located on pg. 122 of the PENTRAN manual.

PENMSHXP Manual [7]

In order for PENTRAN to perform neutron transport equations, it requires a geometry over which to calculate. This geometry could be entered manually into the PENTRAN execution file, but it would be difficult as there would be no way to visualize the geometry. As a result of this dilemma, Dr. Glenn E. Sjoden wrote a program capable of generating a visualization of the programmed geometry and creating a PENTRAN

input deck that automatically populates with the desired geometry. This program is called PENMSHXP, and when PENMSHXP is executed, it makes a series of .png files that display the geometrical details the user has specified. [7] The PENMSHXP manual details the use of the program PENMSHXP which was used to generate a series of input decks for various configurations of the WSMR FBR. PENMSHXP allows for the specification of the level of detail in the x, y, and z directions for a model. Additionally, this manual proved instrumental in creating the reactor components and placing them at the proper locations on each mesh. With PENMSHXP, it is possible to create a myriad of geometric shapes to represent reactor components. For example, it is possible to create a cylinder of any desired diameter to represent a control rod, or a triangle to model the slit of an air flow groove in a fuel assembly. These geometric shapes which are used to represent various reactor components are referred to as “overlays”. These overlays lay over the material of a coarse mesh. The term coarse mesh refers to a block in the x and y direction. These coarse meshes make up the PENMSHXP model, and any number of coarse meshes can be used. It is common to use a symmetric distribution of coarse meshes. For example, a 4x4 PENMSHXP model would consist 16 coarse meshes. Each of these coarse meshes could have multiple overlays, and these overlays could continue from one coarse mesh to the next. It is often desirable to have a number of coarse meshes that is divisible by multiple whole numbers so that they can be distributed across multiple processors with ease. While this manual is not a published journal article or conference paper, the information held within made this research effort possible.

Neutral Particle Transport Theory

Neutral particle interactions with matter are controlled by several variables. First, the energy of the particle must be considered. With a specific energy in mind the next consideration is the material through which the particle will be travelling. Once the energy of the particle and the material that the particle is traveling through has been identified, nuclear cross-section data is accounted for.

A nuclear cross-section is the area presented for interaction by a target nucleus for a specific particle type and energy [8]. These are often split up into three energy regions for each type of particle. These energy regions are commonly referred to as “thermal” (approximately below 1 electron volt (eV)), “epithermal” (1 eV to several keV), and “fast” (several keV to MeV) spectrums. [8]. For this research effort, the primary particle type of interest is the neutron, and the primary energy spectrum is the “fast” region. Neutrons were chosen because the exposure of electronics to neutrons is a common experiment performed at the WSMR FBR, and the fast region was selected because the WSMR operates primarily in the fast region of the neutron energy spectrum. Because the primary neutron energy spectrum is in the fast region, most experiments are interested in exposing test articles to fast neutrons and studying the effects of those interactions. As such, because the goal of this thesis research project was to provide a tool for experimenters to use prior to conducting an experiment at the WSMR FBR, the focus of this research project was to model the fast energy spectrum neutron flux produced during FBR operation.

A PENTRAN user must specify the number of neutron energy groups for the simulation and then provide neutron cross-section data for each material included in the

model at each of those user specified energies. The neutron energies for the Bugle-96 library range from $1e-7$ to 17.332 MeV and are divided into 47 energy groups. Of these 47 energy groups, three are in the thermal region (less than 1 eV), ten are in the epithermal region (1eV to 10 keV), and 34 are in the fast region (10 keV to 17.332 MeV).

In addition to specifying energy groups, A PENTRAN user must specify the number of angles available for scattered particles to assume. The method of specifying these angles is called an S_n method, where n is a number. The number after S , when referring to an angular quadrature scheme, refers to the quadrature level from each trajectory cosine on the unit sphere, where the number of ordinates on the unit sphere is equal to [the number after S plus two] times the number after S . [2] The number after S is commonly referred to as N , and the number of ordinates on the unit sphere is commonly referred to as M . So, as an example, an S_4 discretization has four levels from each direction cosine on the unit sphere, and the number of ordinates on the unit sphere is equal to [four plus two] times four which equals 24. What this means is that for an S_4 calculation the angles that a scattered neutron can assume are restricted to 24 values. As a result of this increase in the number of angles available to model scattering, increases in accuracy compared to real world scattering scenarios (which have a continuum of all angles available as opposed to a discretized set) are often achieved through the use of higher angular discretization schemes. Unfortunately, increasing the number of angles available for scattering adds an ever-increasing number of calculations that need to be performed leading to higher and higher computing resource demands. As such, efforts are usually made to find an optimal angular discretization that achieves the accuracy required for the problem while remaining small enough to be able to be calculated in a timely

manner with the computing resources available. During this analysis and results chapter, only S4 and S8 calculations will be mentioned, while thoughts on higher order discretization schemes will be reserved for the conclusion section of this thesis.

Another PENTRAN parameter that must be chosen by the user is the Legendre Order of the neutron cross-sections. The neutron cross-sections are calculated using a polynomial expansion. When this expansion is performed the answer is truncated after some number of terms. The more terms kept, the greater accuracy of the cross-section, however as the number of kept terms in the cross-section polynomial expansion increases, the time required to execute PENTRAN increases. The Legendre Order is usually expressed as P_n with n being a number indicative of the number of kept terms. Numbering convention starts with P_0 , indicating that only one kept term in the polynomial expansion is used. By comparison, P_1 would have two kept terms from the cross-section polynomial expansion, and P_2 would have three kept terms.

The Boltzmann Transport Equation

This section presents the time-independent source-free transport equation and appropriate boundary conditions. The time-independent form of the equation is used because this research is focusing on steady-state criticality as opposed to an evolution of criticality over some timeframe. The external source-free version was chosen because a geometry change is being induced to begin the fission process as opposed to the introduction of an external neutron source to induce fission. The time-independent external source-free transport equation can be seen in Equation 1. [9]

$$\begin{aligned}
& [\hat{\Omega} \cdot \vec{\nabla} + \sigma(\vec{r}, E)]\psi(\vec{r}, \hat{\Omega}, E) \\
& = \int dE' \int d\Omega' \sigma_s(\vec{r}, E' \rightarrow E, \hat{\Omega}' \cdot \hat{\Omega})\psi(\vec{r}, E', \hat{\Omega}') \\
& + \chi(E) \int dE' \nu \sigma_f(\vec{r}, E') \int d\Omega' \psi(\vec{r}, E', \hat{\Omega}'), \vec{r} \in V
\end{aligned} \tag{1}$$

Equation 1 is a balance equation that provides a means to calculate whether a system of nuclear materials is subcritical, critical, or supercritical. A system that is subcritical is losing more neutrons via absorption and scatter out of the system than are entering the system via scatter back into the system, scatter within the system not resulting in neutron absorption, and neutron production via fission. In contrast, a supercritical system is experiencing a net increase in the neutron population of the system, and a critical system is experiencing neither a net increase nor net decrease in the neutron population of the system. Equation 1 is also used to perform the calculations required to simulate neutron transport through a material. In the context of this research neutrons will be transported through the constituent materials of the WSMR FBR using Equation 1 so that a resultant effective criticality eigenvalue can be obtained.

The boundary conditions chosen when modeling neutron transport have a significant impact on the criticality of the system. In PENTRAN boundary conditions can be set to reflective or absorptive. Reflective boundary conditions force neutrons that would otherwise leave the system (i.e. neutron leakage) back into the system to simulate an infinite boundary in that direction. This artificially increases the effective criticality of the system. By comparison, an absorptive boundary allows neutrons to leave the system (i.e. in-scatter is prevented). This decreases the effective criticality of the system. While the terms “one dimensional” and “two dimensional” are used to describe the piecewise

development of a representative WSMR FBR model, the “one dimensional” and “two-dimensional” models are actually three dimensional models with reflective boundaries. Ultimately, a configuration of absorptive boundaries was chosen for the “three dimensional” (i.e. no reflective boundaries) WSMR FBR model because fast neutrons leaving the system have a low probability of in-scattering back into the system.

Parallel Processing Theory

The PENTRAN user may be tempted to think one can apply an ever increasing number of processors to a calculation and it will increase the speed that the calculation can be performed near exponentially. This assumption is incorrect. The limiting factor on calculation speed is how well the code can distribute the calculation being performed across the processors tasked to work it. A code which is not “parallelizable” cannot effectively break up the problem it is attempting to solve over multiple processors. This limits the speed up that can be gained from using multiple processors. This phenomenon is expressed as Amdahl’s law which states that the optimal increase in speed of a calculation is constrained by the piece of the problem which cannot be aided by parallel processing. The parallelizability of a code is often referred to as a percentage of the code which can benefit from parallel processing. This percentage directly correlates with the hypothetical speed up limit of that code and is often problem dependent. For example, PENTRAN is between 92% and 98% parallelizable. This high fraction of parallelization means that there is a small part of any PENTRAN problem which cannot see gains from parallel processing. This means that PENTRAN stands to gain significantly from parallel processing. According to Amdahl’s law PENTRAN should be able to see a speed up of

20 times through the use of parallel processing, but in order to realize this speed up the problem must be ran on approximately 5,000 processors. By comparison, a code which is less parallelizable, say 75%, can only be sped up by a factor of 4. This speed up would require 128 processors to be realized, and any processors added to the calculation after this would not provide additional speed up in computation time. [10]

PENTRAN was constructed from the ground up with parallelization in mind and this is responsible for its high percentage of calculations capable of benefitting from parallel processing. This attribute allows PENTRAN to perform flux calculations on very large systems on timescales that consist of minutes or hours instead of days or months which other neutral particle transport programs can take. The ability to spread the program across multiple processors also allows for additional fidelity to be added to the model. On a single processor the limit of fidelity would be tied to the memory required to perform the calculation. However, by being able to spread the problem across multiple processors additional detail can be added to the model. Additionally, the large amount of memory required to run the program can be spread across many processors to reduce the memory required per processor to an amount that fits within the processors capabilities.

Summary

The articles and manuals discussed in this chapter were instrumental in the creation of the PENTRAN model of the WSMR FBR created for this research. Specifically, FBR material composition and reactor component dimensions allowed for a more accurate model to be created. Research into the optimization of multi-group cross-sections by the team at GaTech was instrumental to this research effort because it showed

that there was a way to reduce the number of energy groups necessary to model fast burst reactors. By using fewer energy groups the amount of memory required per processor was reduced. This allowed that “saved” memory per processor to be used to increase the fidelity of the model. Neutral particle transport theory provides a means to solve for an effective criticality eigenvalue. This eigenvalue can then be used to analyze the neutron population of the system. Finally, parallel processing theory provides a maximum expectation of speed up and gives an indication of the number of processors that should be used to achieve maximal efficiency. This prevents so called “trial and error” programming where guesses are made and optimization is attempted in a piecemeal fashion.

III. Methodology

Chapter Overview

The purpose of this chapter is to discuss the path that the research effort took and describe the actions that were taken to attempt to achieve the goals of this thesis research project. First, the development of the one dimensional, two dimensional, and three dimensional models of the WSMR FBR will be described. Next, the process of executing PENTRAN with those models will be discussed in depth. Finally, the process used to generate neutron flux plots and scaling factors for the various PENTRAN runs will be described.

FBR Model Construction

The approach to develop a WSMR FBR model began with a simple model consisting of only 1 dimension with reflective boundaries in all directions except positive x (all particles are forced to remain within the system except those that would leak out in the positive x direction). This model encompassed the five materials in the FBR arranged as a series of blocks of various thicknesses. This 1-D model is shown in Figure 2.

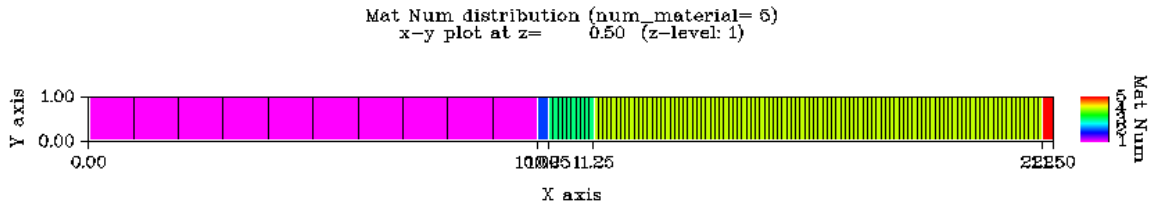


Figure 2. One-Dimensional PENMSHXP FBR Model

This basic model served primarily as a proof of concept and a testbed for features that would be used in the two and three dimensional models. Following development of this model, a number of values were required to be generated prior to executing PENTRAN on the model seen in Figure 2. First, nuclear cross-section data had to be generated. This was accomplished using a program called gmix which receives inputs from the user on the materials and their respective densities and outputs nuclear cross-section data retrieved from the evaluated nuclear data file for a specific set of energies. The Bugle-96 library which was available for this process produced nuclear cross-section data for 47 energy groups for the five materials that make up the WSMR FBR. Gmix also produces several other required values which are necessary to execute PENTRAN or are required for evaluation purposes. Among these are chi values which represent the probability of fission for a material at a specific energy. This means that for each of the five FBR materials, there are 47 chi values (one for each energy group), resulting in a total of 235 chi values. The chi value can be seen in eq. 1 and influences the term responsible for calculating neutron production via fission. Another value generated by gmix is the nu term seen in the neutron production via fission term of eq. 1. Nu represents the number of neutrons produced per fission of an atom of a specific material at a specific energy. Once again, this means that there are 47 values for each material resulting in 235 nu values. The last value generated during the execution of gmix is the energy released per fission of an atom for a specific material. While this term is not used in the execution of PENTRAN, it is used to perform power production analysis. Upon execution of gmix, all values necessary to execute PENTRAN had been obtained. At this point PENTRAN

was executed to gain experience with running PENTRAN and troubleshooting PENTRAN errors as they arose. Simultaneous to this phase of research, the values generated using gmix and the geometry generated using PENMSHXP were sent to Dr. Sjoden, the creator of PENTRAN. He used a technique similar to that used by the GaTech researchers to collapse the 47 energy group cross-sections, chi values, and nu values down to 10 energy groups, chi values, and nu values. This reduced set of values is collectively referred to as the “10 group library” while the original set of values will be referred to as the “47 group library”. This collapsing allowed for PENTRAN to be executed using both the 10 group and 47 group libraries. Once execution of PENTRAN on the PENMSHXP model seen in Figure 2 using both libraries was complete, results were compared to identify similarities and differences that arose when using the two libraries. These initial comparisons yielded nearly identical results which will be discussed further in the Analysis and Results chapter of this thesis document.

After analyzing the one dimensional model a two-dimensional model of the WSMR FBR was constructed. Creating the two dimensional model required the creation of a series of overlays to represent the various reactor components. The first configuration modeled was a 2-D slice through the center of the fuel assembly of the FBR. This configuration was chosen because it best represented the constituent materials of the FBR. The 2-D model representing an x-y plane slice through the FBR at a height of 4.31 cm is shown in Figure 3.

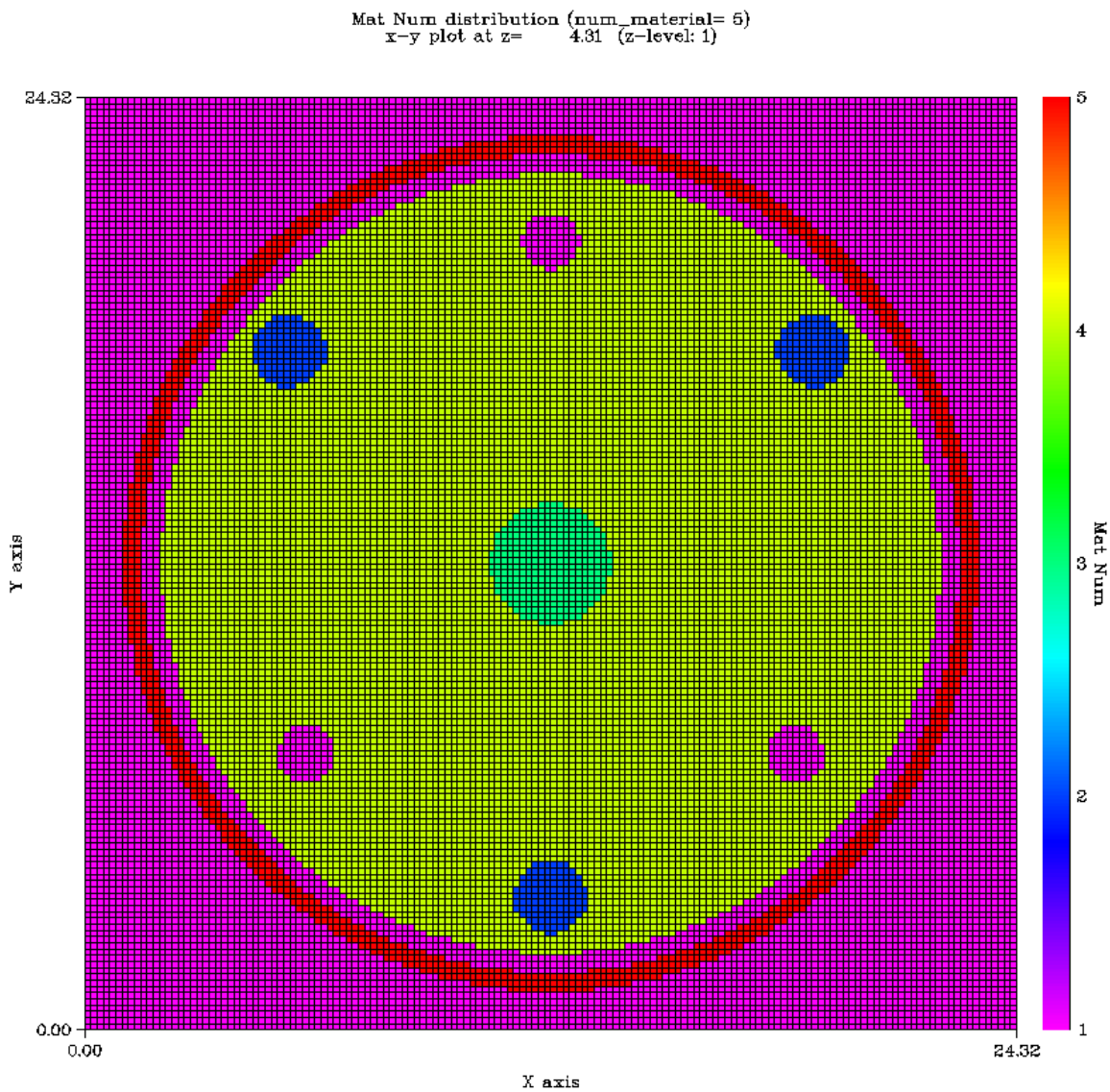


Figure 3: Single Coarse Mesh Two Dimensional FBR Model

The colors in Figure 3 represent the FBR materials. The definition for these materials are described in Table 1. In addition, Table 1 serves as a legend for all the PENTRAN models created during this research effort.

Table 1. Color Legend for WSMR Model Materials

Material	Material Number	Color
Air	1	Pink
Inconel Alloy 625	2	Blue
Stainless Steel 304	3	Green
Uranium/Molybdenum (90/10)	4	Yellow
Boron/Silicon/Carbon (10/50/40)	5	Red

This model does not incorporate multiple coarse meshes which means that this model is not capable of taking advantage of parallel processing by spatially decomposing the coarse meshes across multiple processors. However, this model served as a learning tool on how to create overlays on coarse meshes. As an example of a multiple coarse mesh model, Figure 4 shows a model similar to Figure 3, but it has been divided into 16 coarse meshes.

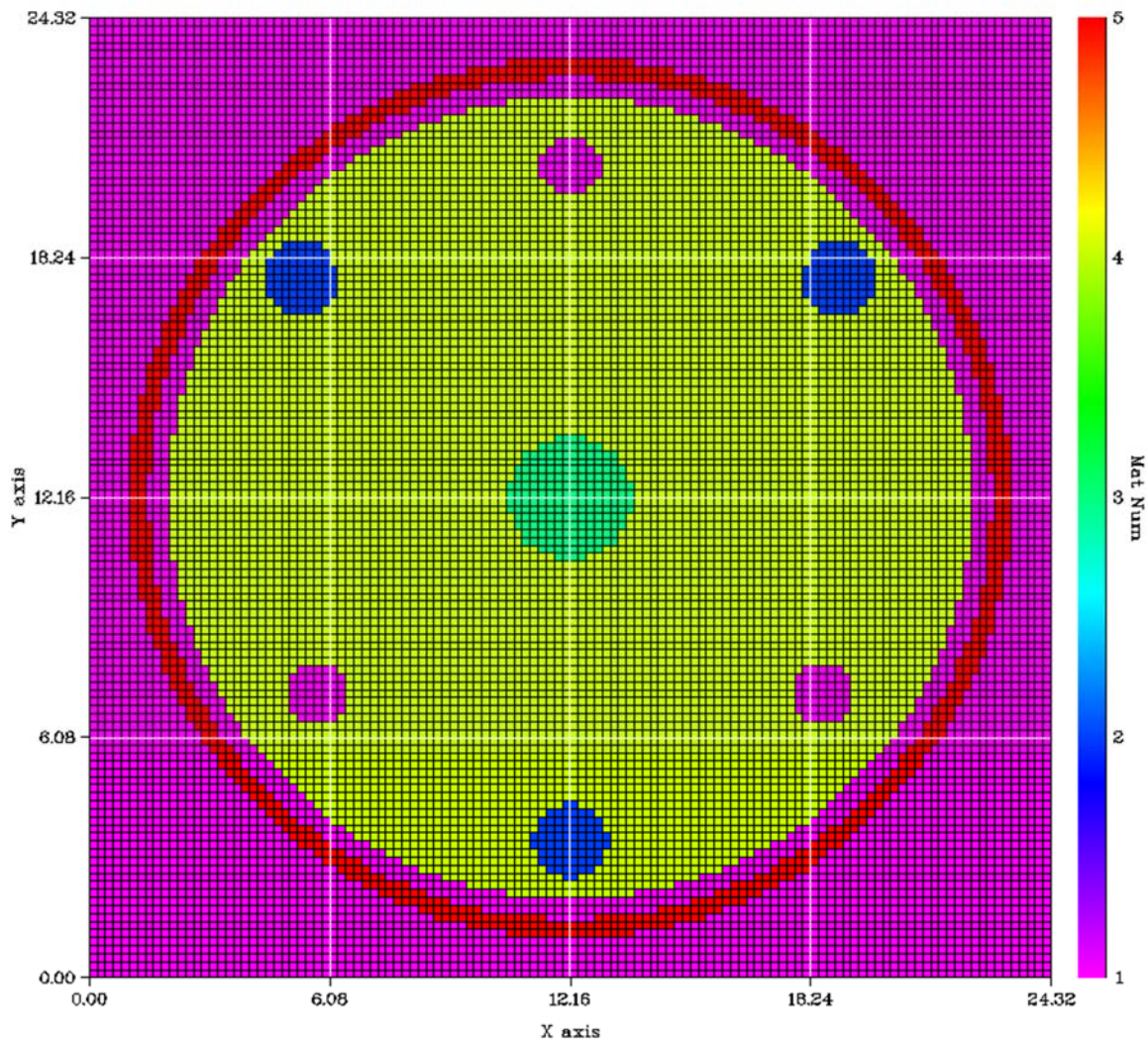


Figure 4. 16 Coarse Mesh Two Dimensional FBR Model

The 2-D models in Figures 3 and 4 show the; air surrounding the boron shroud and between the shroud (in red) and fuel assembly (in yellow). Within the fuel assembly, there are three Inconel bolts which hold the assembly together. A stainless steel core runs vertically through the assembly. Additionally, the WSMR FBR has two control rods and a burst rod. In Figures 3 and 4 these rods have been removed so air appears in the

locations where these rods would be during supercritical operation of the reactor. The dimensions used to create these models are specified in Table 2. This table is a product of combining the dimensions specified in the report “FAST BURST REACTORS IN THE USA” and an engineering analysis performed on Figure 1 which came from that report. Performing an engineering analysis on Figure 1 was required because not all reactor components had their dimensions specified in the “FAST BURST REACTORS IN THE USA” report. A critical assumption made at this point of the research effort was that Figure 1 was drawn to scale, but it is important to note that this may not be true. Table 2 has four columns. The first column calls out specific overlays of reactor components which appear on the PENMSHXP FBR model. The second column indicates where the reactor component overlay begins and ends in the x-direction. For example, an X-Start of 1.00 and X-Stop of 23.32 means that the overlay representing a reactor component begins at 1.00 on the x-axis of the model and ends at 23.32 of the x-axis. The Y-Start and Y-Stop indicate the positions on the Y-axis where the overlay representing the reactor component begins and ends. The Dimensions column is the maximum X and Y distances that the overlays take up. For example, the fuel assembly has dimensions of 22.32 x 22.32; this means that the maximum distance the overlay takes up in the X and Y directions is 22.32 cm.

Table 2. Dimensions Used to Create the WSMR FBR PENTRAN Model

Item	X-Start – X-Stop (cm)	Y-Start – Y-Stop (cm)	Dimensions (cm)
Whole Mesh	0.00 – 24.32	0.00 – 24.32	24.32 x 24.32
Shroud	1.00 – 23.32	1.00 – 23.32	22.32 x 22.32
Air Gap	1.50 – 22.82	1.50 – 22.82	21.32 x 21.32
Fuel Assembly	2.00 – 22.32	2.00 – 22.32	20.32 x 20.32
Inconel Bolt	4.3775 – 6.2825	16.75 – 18.655	1.905 x 1.905
Inconel Bolt	18.0375 – 19.9425	16.75 – 18.655	1.905 x 1.905
Inconel Bolt	11.2075 – 13.1125	2.5 – 4.405	1.905 x 1.905
Control Rod	11.41 – 12.91	19.82 – 21.32	1.50 x 1.50
Control Rod	17.79 – 19.29	6.45 – 7.95	1.50 x 1.50
Burst Rod	5.03 – 6.53	6.45 – 7.95	1.50 x 1.50
Steel Core	10.5725 – 13.7475	10.5725 – 13.7475	3.175 x 3.175

Once the initial 16 coarse mesh two dimensional model shown in Figure 4 was created, a series of criticality experiments were performed with this model in different configurations. The configurations included the following: the original configuration in Figure 4, the control and burst rods fully inserted, and finally the control and burst rods as well as the safety block removed. The safety block is a 10.16 cm cylinder that is centered at the center of model. A version of the model with the safety block and control and burst rods removed can be seen in Figure 5.

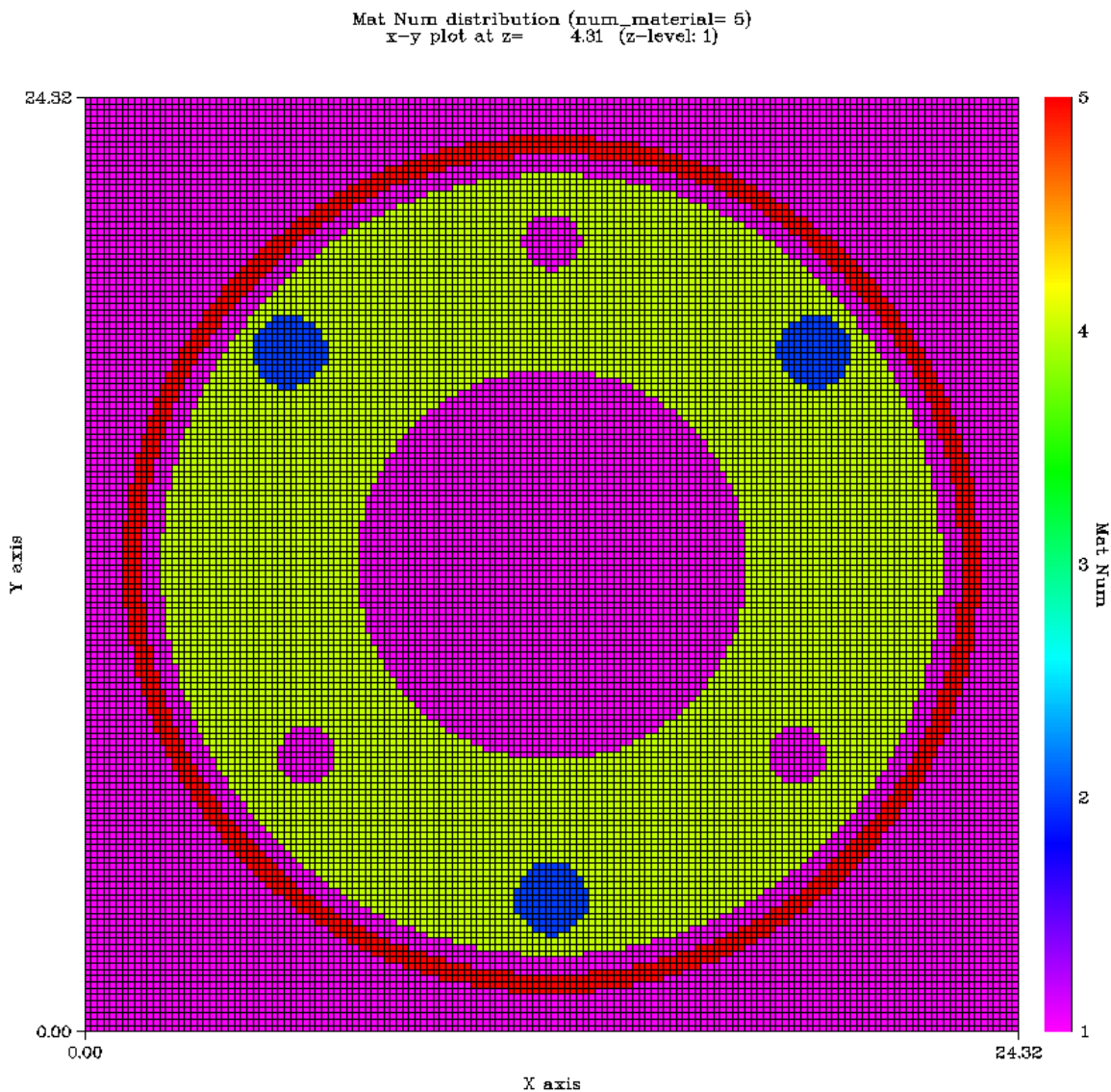


Figure 5. FBR Model with Safety Block, Burst Rod, and Control Rods Removed

The purpose of the safety block is to render the system subcritical if the safety block is not inserted. PENTRAN calculations were performed on the model without the safety block inserted to ensure that PENTRAN would return subcritical results.

PENTRAN calculations confirmed that the geometry modeled in Figure 5 returned a subcritical system. As with the one-dimensional model, comparisons were made when

running PENTRAN with the Bugle-96 library and 10 group collapsed library. Unlike parameter studies conducted on the one-dimensional model, different quadrature schemes (S4, S8) were performed on the two-dimensional model. The detailed results of these parameter studies are discussed in the next chapter.

Following the analysis on the two-dimensional model, preparations were made to move from one z-level to a series of z-levels to form a three-dimensional model of the WSMR FBR. Moving to a three-dimensional model required a decision on the number of z-levels needed to accurately represent the FBR. This required an additional decision as to which FBR configuration to model. A steady state reactor operation with the control and burst rods removed was modeled. Table 3 shows the z-level dimensions used for three dimensional WSMR FBR construction. These dimensions were chosen by examining Figure 1 and identifying the number of z direction unique instances existed. For example, Figure 1 shows the burst rod not extending as far as the control rods. Because model geometry in the z-direction has changed a new z-level is required to represent this change. By analyzing Figure 1, 6 unique z direction instances were identified and as a result 6 z-levels were necessary to represent the FBR in PENMSHXP.

Table 3. Z-Level Dimensions for WSMR FBR Model

Z-Level	Z-Level Start (cm)	Z-Level Stop (cm)
1	0.0	1.27
2	1.27	14.19606
3	14.19606	17.4117
4	17.4117	20.32
5	20.32	20.955
6	20.955	22.225

Six two dimensional x-y plane slices representing the six z-levels that were created using PENMSHXP are shown in Figures 6 through Figures 11.

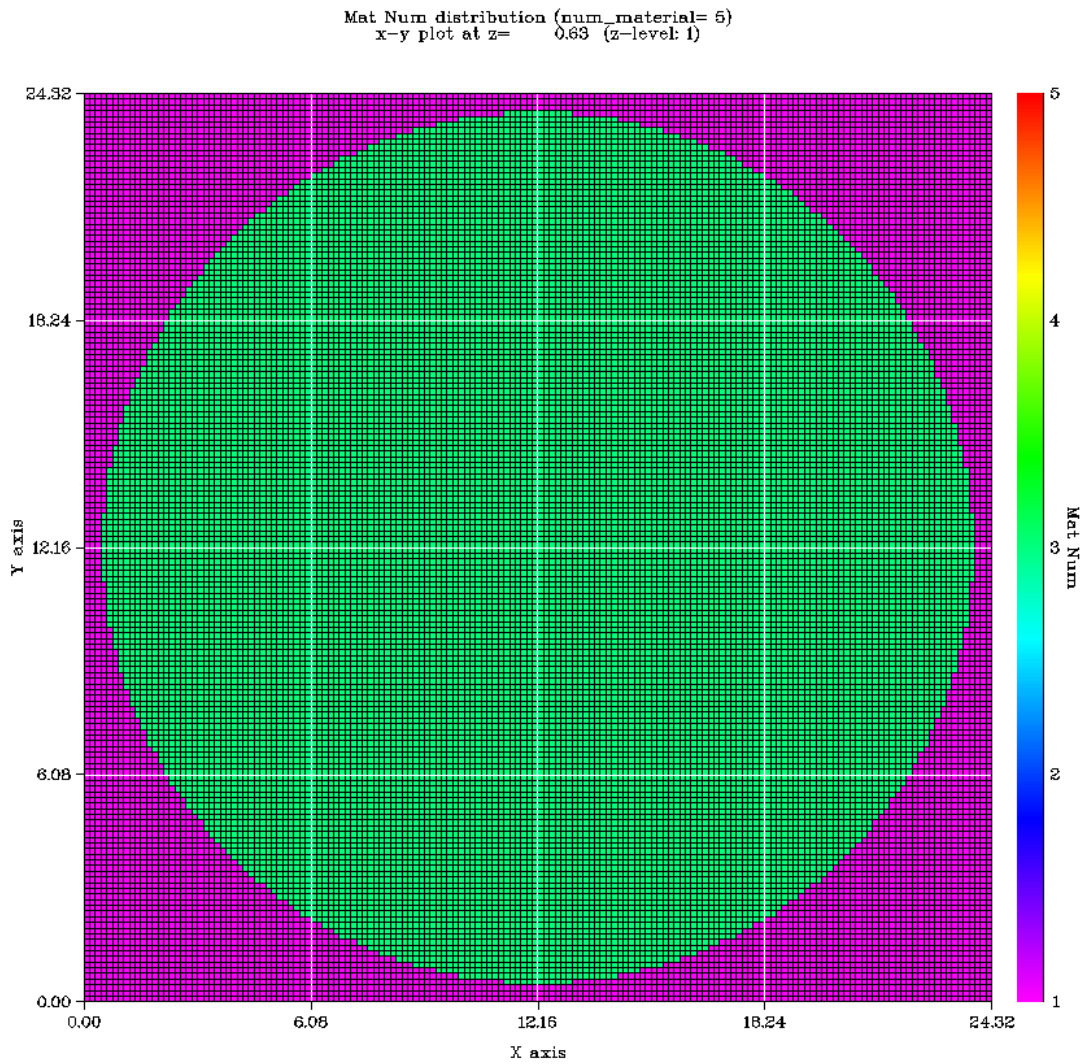


Figure 6. Z-Level One WSMR FBR Model

Z-level one represents the bottom of the WSMR FBR with the safety block fully inserted. This z-level models the stainless steel support plate, shown in Figure 1, upon which the fuel assembly sits.

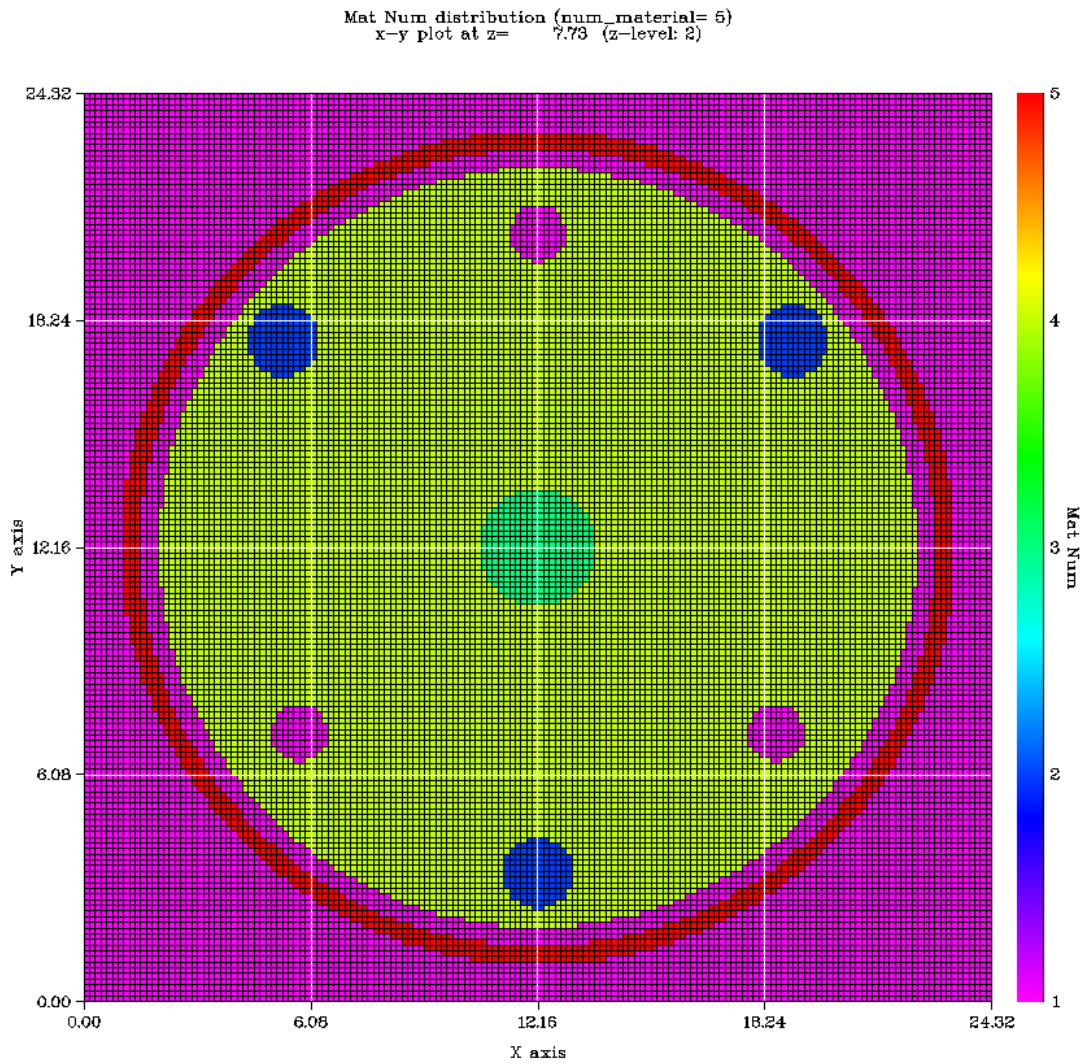


Figure 7. Z-Level Two WSMR FBR Model

Z-level two is similar to the mesh displayed in Figure 4. This z-level, models the same features described on that mesh which were mentioned earlier in this chapter.

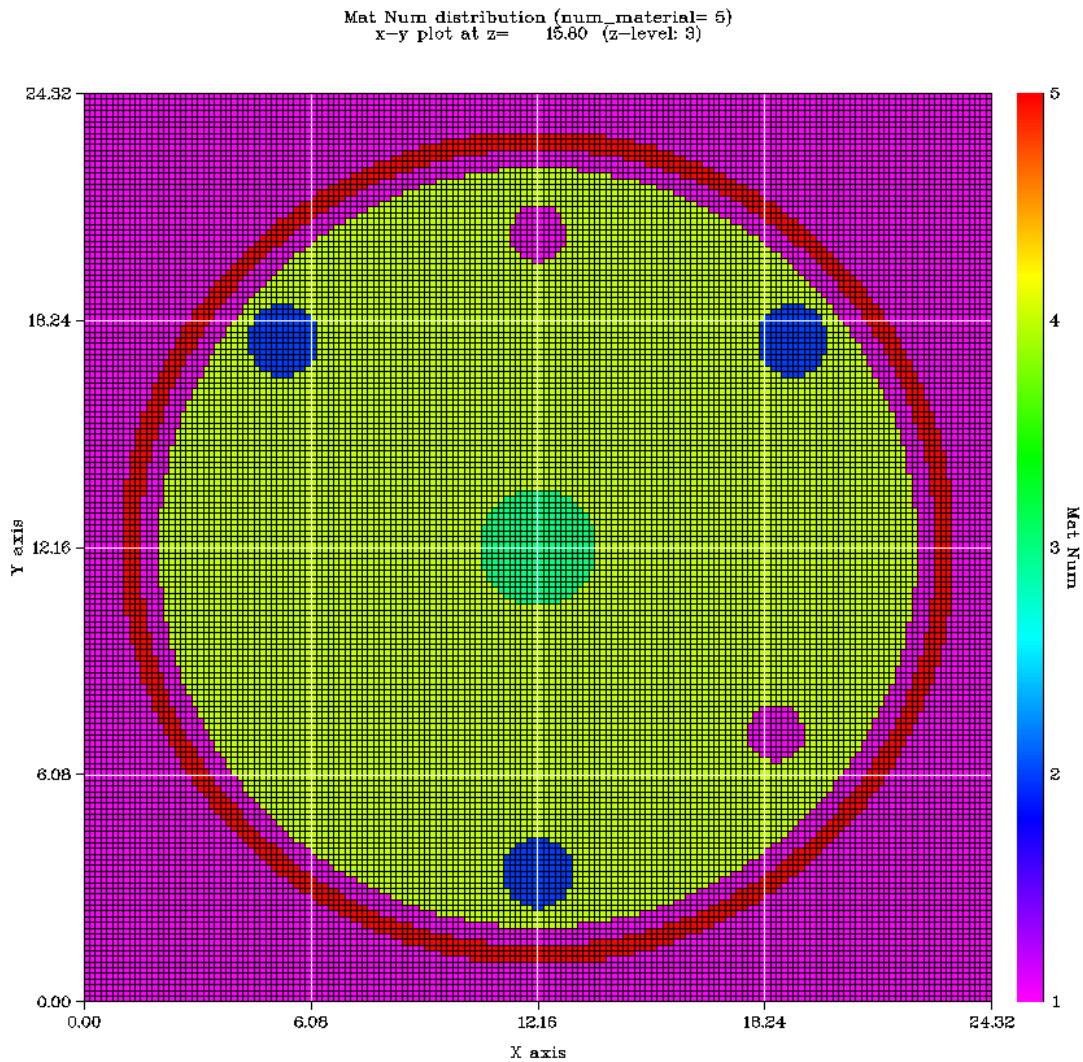


Figure 8. Z-Level Three WSMR FBR Model

Z-level three has most of the key features seen in z-level two. However, the burst rod does not extend in the z direction as far as the two control rods. To model this geometry, the burst rod shown in z-level two in Figure 7 is replaced by fuel in z-level three shown in Figure 8.

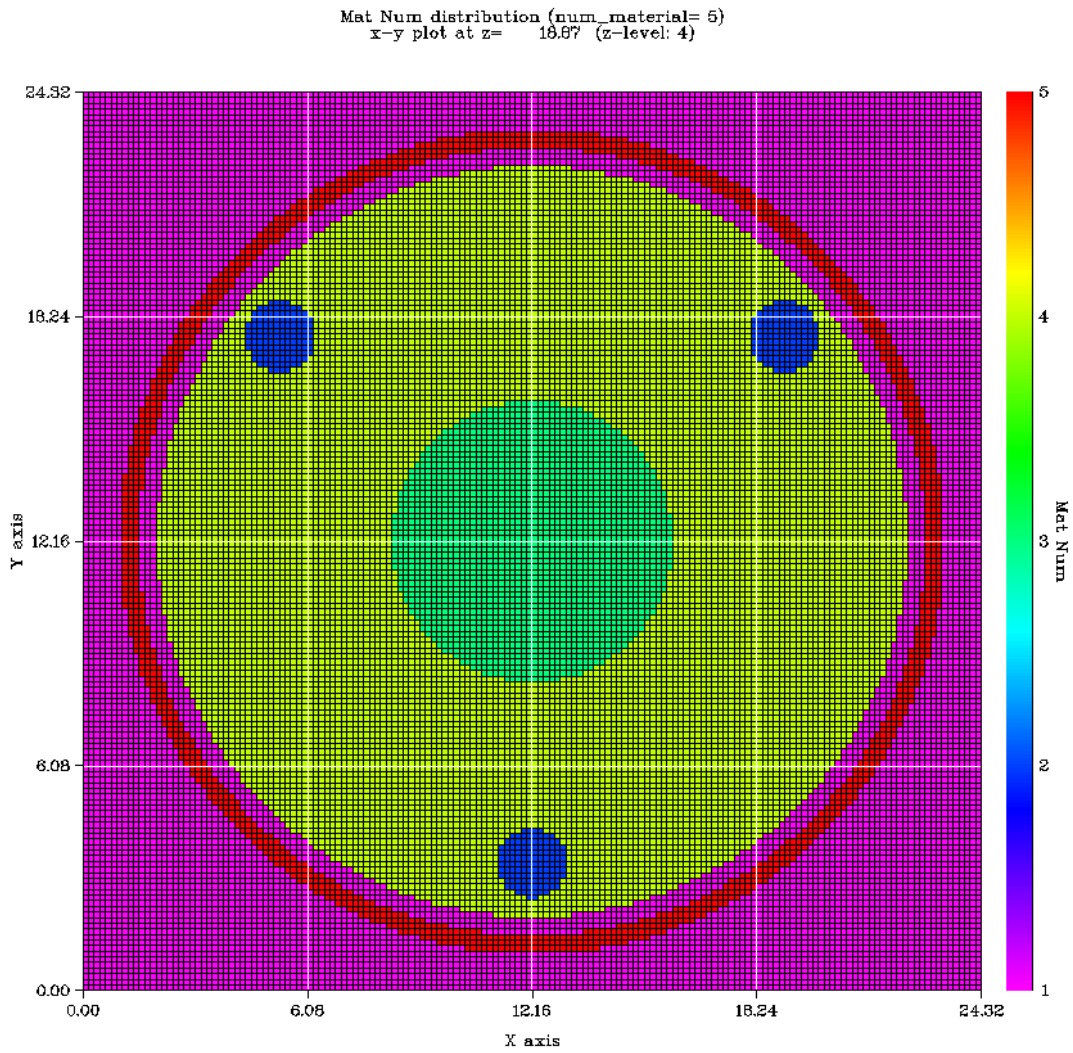


Figure 9. Z-Level Four WSMR FBR Model

Z-level four is the final z-level of the fuel assembly. As can be seen, the control rods do not extend vertically into this z-level. Instead, the steel core at the center of the mesh is replaced by a larger stainless steel mass adjustment ring at the center of this z-level.

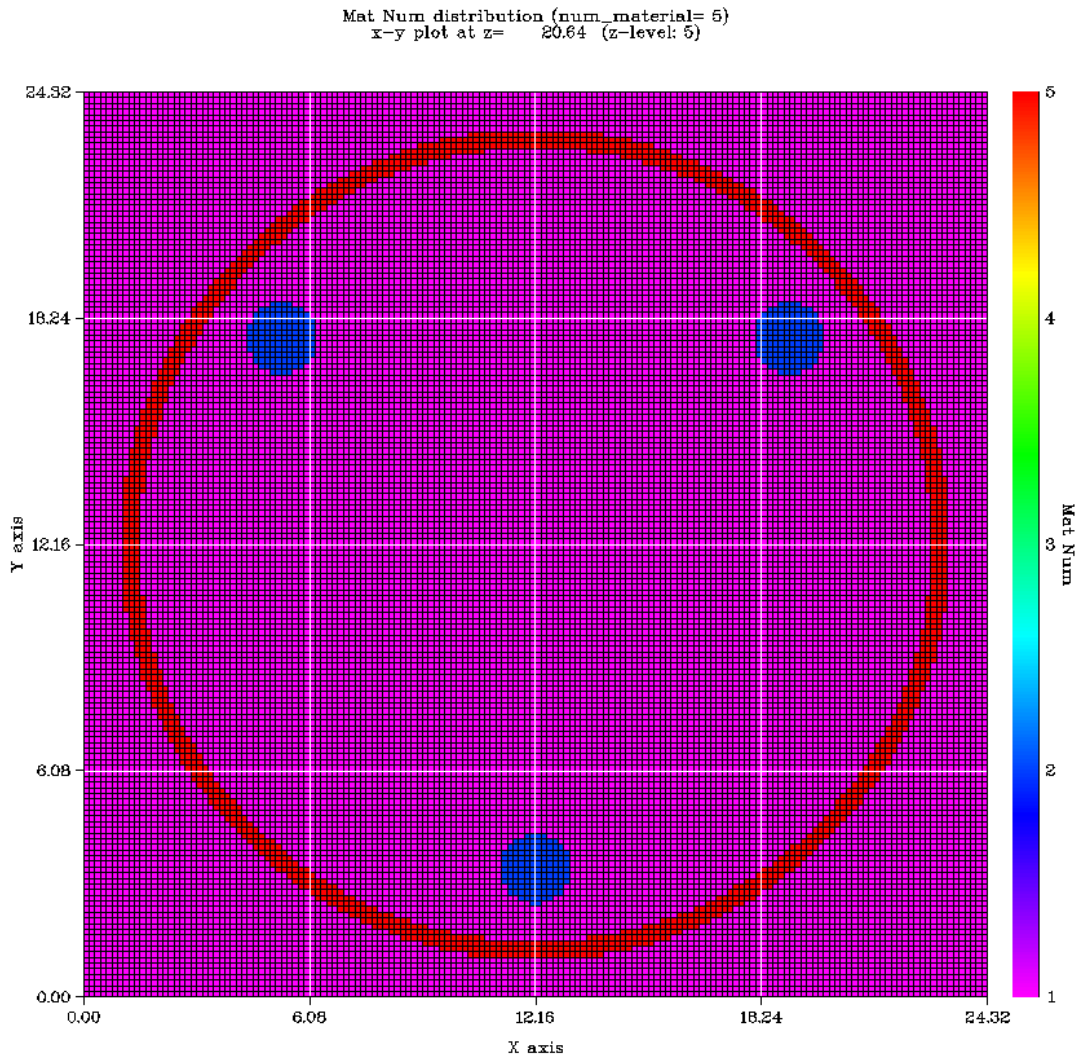


Figure 10. Z-Level Five WSMR FBR Model

Z-level five represents an x-y slice of the FBR immediately above the fuel assembly. In this z-level only the Inconel bolts which extend beyond the fuel assembly, the boron shroud, and the air in between these components are present.

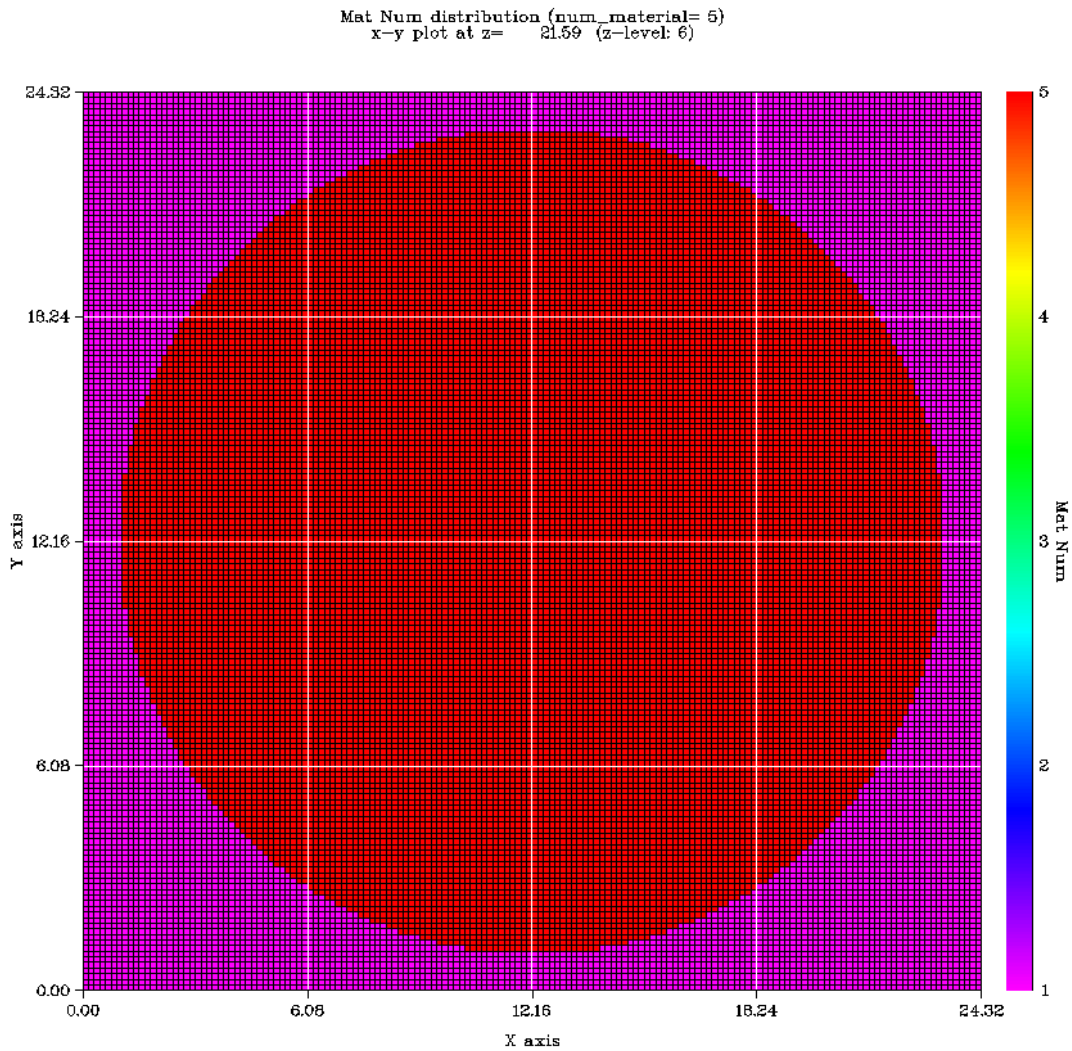


Figure 11. Z-Level Six WSMR FBR Model

The final z-level, six, represents a slice through the top of the boron shroud. This z-level only contains boron and air.

Once the three dimensional FBR model was created, flux calculations could be performed with PENTRAN for different quadrature levels (S4, S8), Legendre orders (P0, P1, and P2), and different neutron cross-section libraries (Bugle-96 47 group and collapsed 10 group). The available PENTRAN parameters resulted in 12 potential

combinations of PENTRAN simulations. Ten calculations of these 12 possible combinations were performed using the Air Force Research Laboratory (AFRL) DoD Supercomputing Resource Center (DSRC). Two of the 12 were not able to be executed due to numerical instabilities in the DSRC system for PENTRAN. This computing resource allowed for the tasking of more processors than were available on AFITs machines. This tasking of many processors was required due to the large amount of memory needed to perform flux calculations on complex geometries such as the three dimensional WSMR FBR model created for this research effort. Additionally, as was discussed in chapter two of this thesis, reaching maximum theoretical speedup for a code that is between 92% and 98% parallelizable would require several thousand processors. Due to computational resource constraints, only hundreds of processors were used in lieu of thousands, but the speed up achieved still allowed the problem to be worked in a matter of hours as opposed to days or weeks. The results of these PENTRAN runs will be discussed in detail in the next chapter.

Additionally, with the model fully created, an analysis could be performed to compare the actual masses of each material in the FBR to the mass of each material in the model. PENMSHXP automatically calculates the mass of each material in the model and compares it to user specified target masses. Thus, a target amount of each material is specified before the model is generated, and upon model creation, a file will be created comparing the target and model material amounts. How the target and model material masses compared will be further explored in the next chapter.

Summary

This chapter has described the process of the constructing the FBR PENTRAN model from a simple one z-level model to a multi-z-level 3-D model with the appropriate reactor dimensions. The process began with a single diagram and a brief description from Thomas F. Wimett's "FAST BURST REACTORS IN THE U.S.A", and concluded with a PENMSHXP model consisting of six z-levels and a model that can continue to be improved in the future.

IV. Analysis and Results

Chapter Overview

The purpose of this chapter is to present the results of this research. Additionally, the differences and similarities between different PENTRAN run configurations are analyzed. Primary focus is on examining differences in flux values arising from using different discretization schemes and cross-section libraries. Comparisons are made between PENTRAN and MCNP flux predictions and k effective values.

Simulation Results

Chapter three discussed the creation of a representative PENMSHXP model of the FBR. Once the PENMSXHP model was completed, flux calculations could be performed using PENTRAN. The following ten runs were performed: an S4 calculation using the Bugle-96 47 group, an S4 calculation using the collapsed 10 group version of the Bugle-96 library, and S8 calculations for each cross-section library. Additionally, PENTRAN runs were performed using different Legendre order (P-order) cross-section data. These different P-order runs were performed for all combinations of S-orders and libraries with the exception of Bugle-96 S8 P1 and Bugle-96 S8 P2 runs. As discussed above, these runs were not performed due to instabilities on the DSRC system which caused the calculation to diverge. The energy group upper limits used in these two libraries are shown in Tables 4 and 5.

Table 4. Energy Groups Used in the 47 Group Bugle-96 Library

Energy Group	Upper Energy (MeV)
1	17.332
2	14.191
3	12.214
4	10.000

5	8.6071
6	7.4082
7	6.0653
8	4.9659
9	3.6788
10	3.0119
11	2.7253
12	2.466
13	2.3653
14	2.3457
15	2.2313
16	1.9205
17	1.653
18	1.3534
19	1.0026
20	0.82085
21	0.74274
22	0.6081
23	0.49787
24	0.36883
25	0.29721
26	0.18316
27	0.11109
28	0.067379
29	0.040868
30	0.031828
31	0.026058
32	0.024176
33	0.021875
34	0.015034
35	0.0071017
36	0.0033546
37	0.0015846
38	0.000454
39	0.00021445
40	0.0001013
41	0.000037266
42	0.000010677
43	0.0000050435
44	0.0000018554
45	0.00000087643
46	0.00000041399
47	0.0000001

Table 5. Energy Groups Used in the Collapsed 10 Group Version of the Bugle-96 Library

Energy Group	Upper Energy (MeV)
1	17.332
2	3.6788
3	1.653
4	0.82085
5	0.6081
6	0.36883
7	0.11109
8	0.0071017
9	0.0000050435
10	0.0000001

When PENTRAN performs a calculation, it generates a series of flux files containing information for each energy group and z-level that was specified in the PENTRAN execution file. These flux files can then be used by PENMSHXP to generate flux plots for a given location on each coarse mesh for each energy group. As an example, the flux plot of z-level two for energy Group 17 of the Bugle-96 47 group library (1.3534-1.653 MeV) for an S8 P0 run can be seen in Figure 12. Because high energy neutrons are the primary interest at the WSMR FBR, the primary energy group that will be used to compare across various PENTRAN runs is 1.3534-1.653 MeV. This energy appears in both cross-section libraries, and is group 17 in the Bugle-96 47-group library, and group three in the collapsed 10 group library. The most often analyzed z-level will be z-level two because it contains the most adjustable objects (two control rods and a burst rod). Comparisons will also be made about the criticality of the various PENTRAN runs.

Flux distribution for group=17
x-y LOG plot at z= 7.73 (z-level: 2)

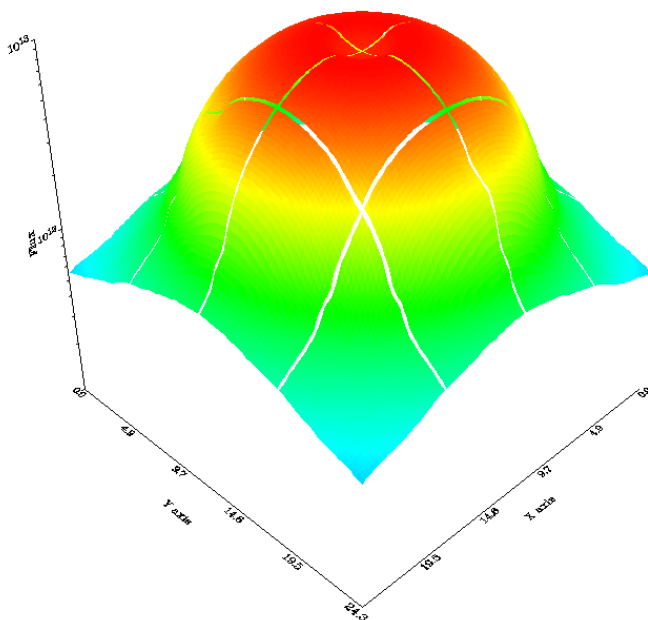


Figure 12. Z-Level Two S8 P0 G 17 Bugle-96 Library (1.3534-1.653 MeV) Flux Plot

The magnitude of the neutron flux in Figure 12 is on the vertical axis reaching about 10^{13} neutrons/cm² in the center of the mesh. Figure 12 is an x-y slice at $z=7.73$ cm (the center of z-level 2). The x and y coordinates are the length and width of the z-level that the plot is representing. At this point, it might seem logical to present a series of flux plots with the same energy group for the same z-level while changing the discretization scheme and cross-section library used during flux calculations. As an example of the similarity in flux values predicted by PENTRAN when using the same cross-section library but different discretization schemes, Figure 13 shows a flux plot from an S4 P0 Bugle-96 run for the same energy group and z-level as Figure 12.

Flux distribution for group=17
x-y LOG plot at z= 7.78 (z-level: 2)

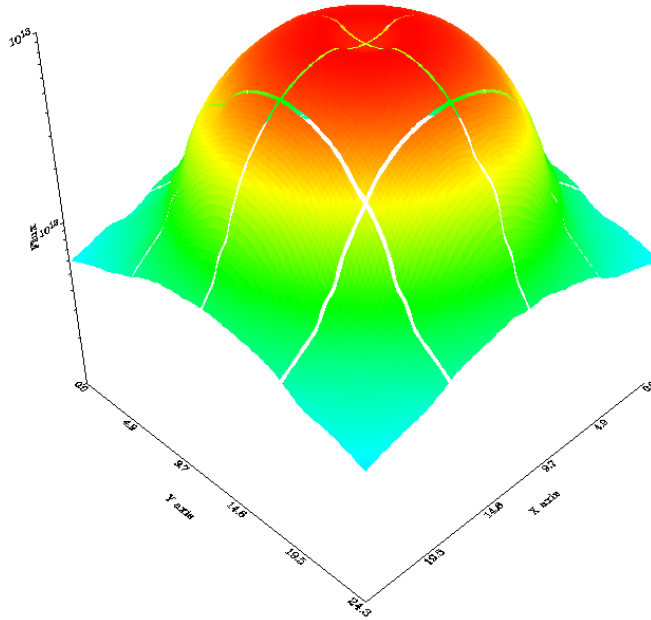


Figure 13. Z-Level Two S4 P0 G 17 of Bugle-96 Library (1.3534-1.653 MeV) Flux Plot

Figures 12 and 13 appear nearly identical. It would be repetitive to present a flux plot for each energy group. The remainder of the flux plots appear identical when comparing an S4 run versus an S8 run while using the same cross-section library. Because most of the neutrons created in the system are high energy neutrons, and high energy neutrons have a low probability of interacting with the material of the FBR, the probability of scatter is low, which results in few scatter events. The low amount of scatter means that the 24 angles allowed by an S4 calculation are sufficient to capture the effects of scatter at the WSMR FBR and adding additional angles such as the 80 present in an S8 calculation does not provide much improvement to the simulation results.

Changing the quadrature level, while keeping the cross-section library the same between S4 and S8, did not appear to influence the k_{eff} of the system significantly. k_{eff} is calculated by assuming that the number of neutrons released during any fission event can be modified to reach a time-independent solution to Equation 1. When $k_{\text{eff}}=1$ the system is critical, greater than 1 means the system is supercritical, and if k_{eff} is less than 1 the system is subcritical. The k_{eff} calculated in each PENTRAN run is shown in Table 6.

Table 6. Criticalities of PENTRAN/MCNP Runs

PENTRAN Run	k-effective
S4 P0 Bugle-96	1.209 +/- 1.9e-5
S4 P0 10 Group	1.206 +/- 2.5e-5
S8 P0 Bugle-96	1.212 +/- 1.3e-5
S8 P0 10 Group	1.209 +/- 1.9e-5
S4 P1 Bugle-96	1.101 +/- 4.3e-5
S4 P1 10 Group	1.100 +/- 8.6e-5
S8 P1 10 Group	1.102 +/- 7.1e-5
S4 P2 Bugle-96	1.105 +/- 1.1e-5
S4 P2 10 Group	1.102 +/- 3.1e-5
S8 P2 10 Group	1.105 +/- 3.0e-5
MCNP Run	Combined 1.096 +/- 6.3e-4
MCNP Run	Collision 1.096 +/- 7.2e-4
MCNP Run	Absorption 1.096 +/- 7.1e-4
MCNP Run	Track-Length 1.096 +/- 6.6e-4

Significant differences arise when comparing K-effectives calculated using identical quadrature levels but different cross-section Legendre orders. This can be seen in Table 6 where the P0 runs all yield k_{eff} significantly higher than P1 or P2 runs. A significant challenge was discerning which of these results was the most accurate. P1 and P2 PENTRAN runs should result in a better model due to the increased accuracy when modeling the scattering term of Equation 1. This increased accuracy comes from the additional terms kept in the polynomial expansion of the cross-sections. The modeled FBR configuration should be less than 1 since both control rods and the burst rod are

removed, this indicates the model has extra fuel. At this point it will be useful to present a bit of work performed by the advisor of this thesis research effort.

Lt Col James Fee created an MCNP FBR model using the same dimensions specified in Table 2. A cutaway of this model can be seen in Figure 14.

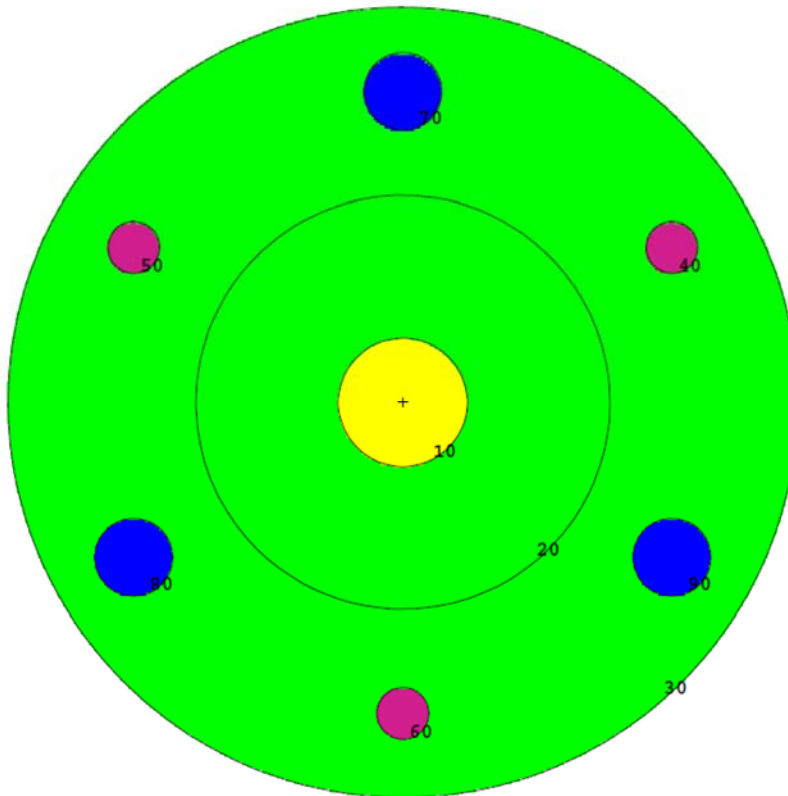


Figure 14. Lt Col James Fee's MCNP FBR Model

Lt Col Fee performed a criticality calculation on the MCNP model seen in Figure 14 and achieved a k_{eff} of 1.09. MCNP uses continuous energy neutron cross-sections as opposed to a discretized set or “library”. While it has already been determined that increasing the number of available angles in the PENTRAN runs had little to no effect, it was clear that the Legendre order of the cross-sections had a substantial impact on the k_{eff} . Because a Monte Carlo method (MCNP) and a discrete ordinates method

(PENTRAN) both calculated a similar k_{eff} when using identical geometries, it is proposed that the PENTRAN runs using the P1 and P2 Legendre order are closer to the “correct” value. These results suggest that the cross-sections of both the Bugle-96 and collapsed 10 group libraries are incapable of representing the neutrons present at the FBR when a P0 Legendre order is used, but when P1 and P2 cross-sections are applied, either library is capable of achieving a k-effective within 2% of the k-effective predicted by MCNP. It is also clear that while the difference between a P0 and P1 run is significant, there is no significant difference between the P1 and P2 runs. This implies that for this problem a Legendre order of P1 is “good enough”, and expending computational resources for P2 runs does not gain accuracy.

Summarizing the trends that surfaced during this research effort leads to the following conclusions: using an S4 or S8 angle discretization scheme had little to no impact on k_{eff} or predicted flux values; using cross-section libraries with different Legendre orders had a significant impact on the k_{eff} and predicted flux values, with the P0 Legendre order over predicting the k_{eff} values of the system; an MCNP model using the same dimensions produced a criticality which agreed with the results of the P1 and P2 PENTRAN runs.

In order to analyze the accuracy of the model for representing the materials in the FBR design, the three dimensional PENTRAN model with regards to the intended creation parameters was examined. This analysis used a mass balance file which is produced when PENMSHXP is run for mesh generation. The information presented in Table 7 shows the model volume which was calculated by PENMSHXP during mesh generation and the target volume which was calculated by hand using the volume

formulas for the various shapes of the FBR components. These calculations were performed for each material and give an estimate of the validity of the model compared to the actual FBR reactor dimensions.

Table 7. WSMR FBR Three Dimensional PENTRAN Material Balance Information

Material	Target Volume (cm ³)	Model Volume (cm ³)	Difference (cm ³)	Model High or Low
Air	5774.134	5339.965	434.169	Low
Inconel	168.321	164.9145	3.4065	Low
Stainless Steel	802.867	802.7696	0.0974	Low
Uranium Molybdenum	5679.54	5677.337	2.203	Low
Boron Loaded Silicate	1172.983	1158.105	14.878	Low

The last column of Table 7 shows that the PENMSHXP calculated model volume was consistently lower than the hand calculated target volume. Round off error is likely a primary cause for the relatively small differences noticed in the final four materials. The air volume being off by 8% is likely to have a slight impact on the system criticality. The material taking the place of that air will have a much larger impact to the system criticality, particularly if it is fuel. Why the target and model air volumes have such a large difference between the two is not immediately apparent. The final four rows in Table 7 show the model volumes are within two percent or less of their respective target volumes, but the air model volume differs from the target volume by about eight percent. The method by which the air target volume was calculated could be the cause. The air volume was calculated by using the target air volume with no other materials present and then subtracting each of the remaining materials from that total air volume. A portion of one of the other materials not being subtracted properly is a potential cause for the greater difference between target and model air volumes compared to the other model materials.

The materials that represent the components of the FBR are all within two percent of their hand calculated target volumes, which gives confidence that PENMSHXP is representing the reactor accurately. Unfortunately, due to difficulty in obtaining the exact FBR dimensions, it is difficult to say with any degree of certainty the accuracy when compared to the exact FBR dimensions. However, it can be said that the model is representative of the dimensions chosen to represent the WSMR FBR. Any error arising from assumptions made when determining those dimensions would inevitably propagate into both the target and model volumes. Under ideal circumstances a third column would be included in Table 7 showing what the exact FBR volumes were and comparisons would be made to those values as well, but until dimensional can be obtained regarding the FBR, such observations cannot be made.

Leakage Analysis

A leakage analysis was performed on the S4 P1 10 Group PENTRAN run to identify where leakage was occurring throughout the system. The leakage from the six surfaces which bound the system were examined and the leakage through each of those surfaces was further scrutinized based on the energy group that the particle was in when it leaked out of the system. If the system behaved as would be expected, there should be significantly less leakage in the thermal group than in the fast groups. Less leakage in the thermal group is expected because the boron-loaded silicate shroud has a high probability of absorbing the thermal neutrons before they reach the edges of the system where they can leak out. Leakage from the S4 P1 10 Group PENTRAN run is shown in Table 8.

Table 8. Neutron Leakage [$\text{n}/\text{cm}^2 \cdot \text{s}$] for S4 P1 10 Group PENTRAN Run

Group	-x	+x	-y	+y	-z	+z
1	2.7e14	2.7e14	2.7e14	2.7e14	2.7e14	2.5e14
2	8.9e14	8.9e14	8.8e14	8.9e14	9.4e14	8.3e14
3	1.0e15	1.0e15	9.9e14	9.9e14	1.1e15	9.4e14
4	4.3e14	4.3e14	4.3e14	4.3e14	5.0e14	4.1e14
5	6.0e14	6.0e14	6.0e14	6.0e14	6.9e14	5.6e14
6	6.7e14	6.7e14	6.6e14	6.7e14	7.6e14	6.4e14
7	1.7e14	1.7e14	1.7e14	1.7e14	1.7e14	1.7e14
8	9.3e11	9.3e11	9.4e11	9.4e11	1.3e12	1.0e12
9	2.1e6	2.1e6	2.1e6	2.1e6	1.6e7	4.2e5
10	1.1e4	1.1e4	1.1e4	1.1e4	1.2e5	1.9e3
Total	4.0e15	4.0e15	4.0e15	4.0e15	4.5e15	3.8e15

The $-x$, $+x$, $-y$, $+y$, $-z$, and $+z$ indicate which face of the square prism makes up the three-dimensional model the neutrons are leaking out of. As shown in Table 8, Group 10 (the thermal group) is contributing the least to leakage because neutrons in this energy range are preferentially absorbed by the boron-loaded silicate shroud. Additionally, the majority of the neutrons generated in this simulation are born fast and would have to undergo significant moderation to reach the thermal energy group. As a result, the combination of preferred absorption by the shroud and fewer neutrons being moderated into the thermal group leads to fewer thermal neutrons reaching the edge of the model. The lower number of thermal neutrons reaching the edge of the model results in fewer thermal neutrons leaking out of the system. The thermal group leakage is approximately ten orders of magnitude lower than leakage from the non-thermal groups.

Flux Scaling Factors

While k_{eff} between various PENTRAN runs can be compared directly, a scaling factor must be used to compare flux plots between different PENTRAN runs. This scaling factor is the factor that the current power level of the reactor model must be multiplied by to reach a target power amount. In this case 0.008 Megawatts (MW) was chosen because that is the operating power that the FBR runs at when in steady-state mode. By scaling the fluxes, direct comparisons can be made between flux plots of different PENTRAN runs. The flux scaling factors associated with each PENTRAN run to get to 0.008 MW are shown in Table 9.

Table 9. Flux Scaling Factors

PENTRAN Run	Flux Scaling Factor
S4 P0 Bugle-96	1.53735e-02
S4 P0 10 Group	9.71518e-03
S8 P0 Bugle-96	1.14767e-02
S8 P0 10 Group	9.69130e-03
S4 P1 Bugle-96	1.18964e-02
S4 P1 10 Group	1.24725e-02
S8 P1 10 Group	1.24384e-02
S4 P2 Bugle-96	Not Obtained
S4 P2 10 Group	1.24144e-02
S8 P2 10 Group	1.23278e-02

Model Refinement

Because PENTRAN was over-predicting the k_{eff} of the system for the configuration chosen, there was a desire to add air flow grooves to the PENMSHXP model to see if the k_{eff} would be reduced significantly. A PENTRAN k_{eff} calculation was performed for the S4 P1 10 Group PENTRAN parameters as those parameters had

yielded the closest results to the analogous MCNP simulation. The air flow grooves only appear in z-levels two and three, and these new z-levels are shown in Figures 15 and 16.

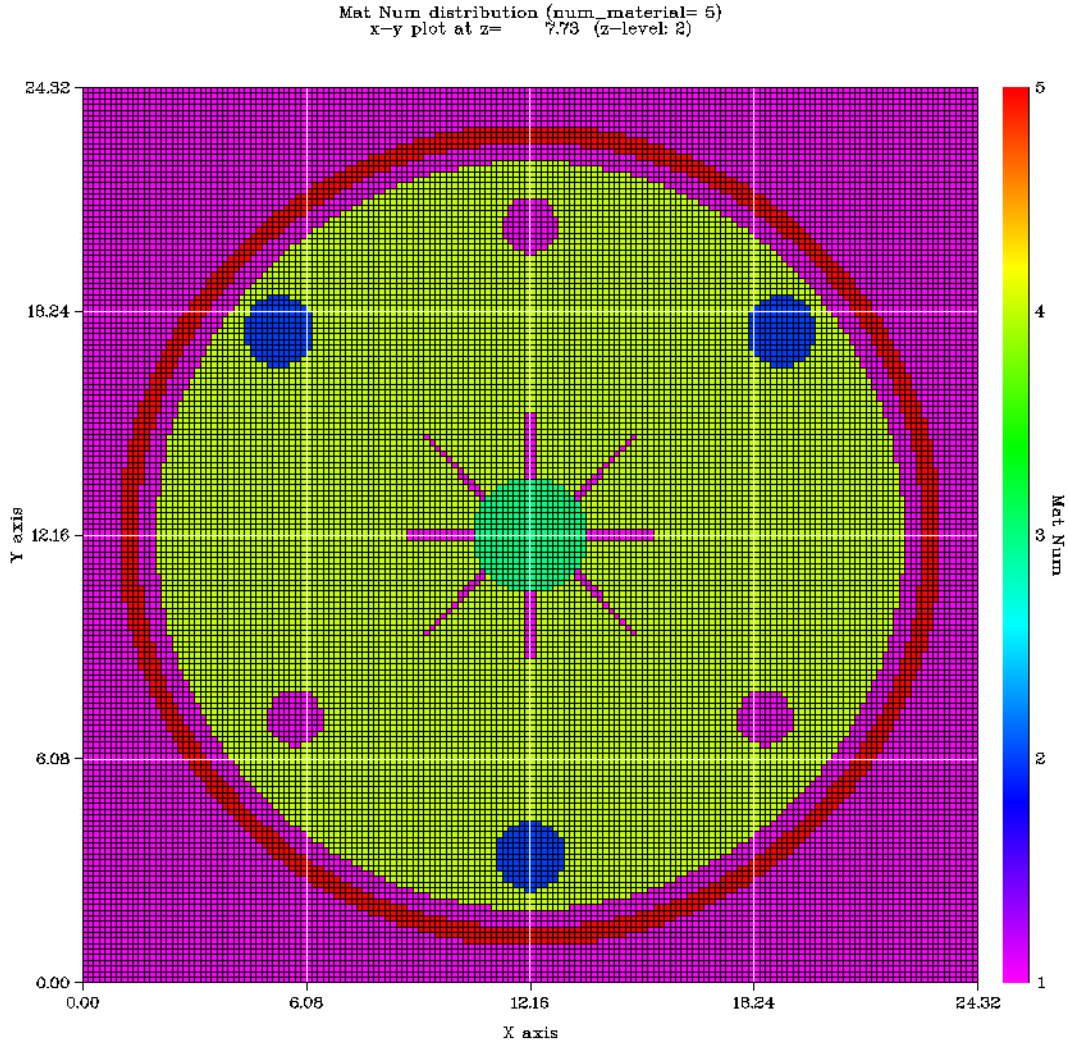


Figure 15. Z-Level Two with Air Flow Grooves

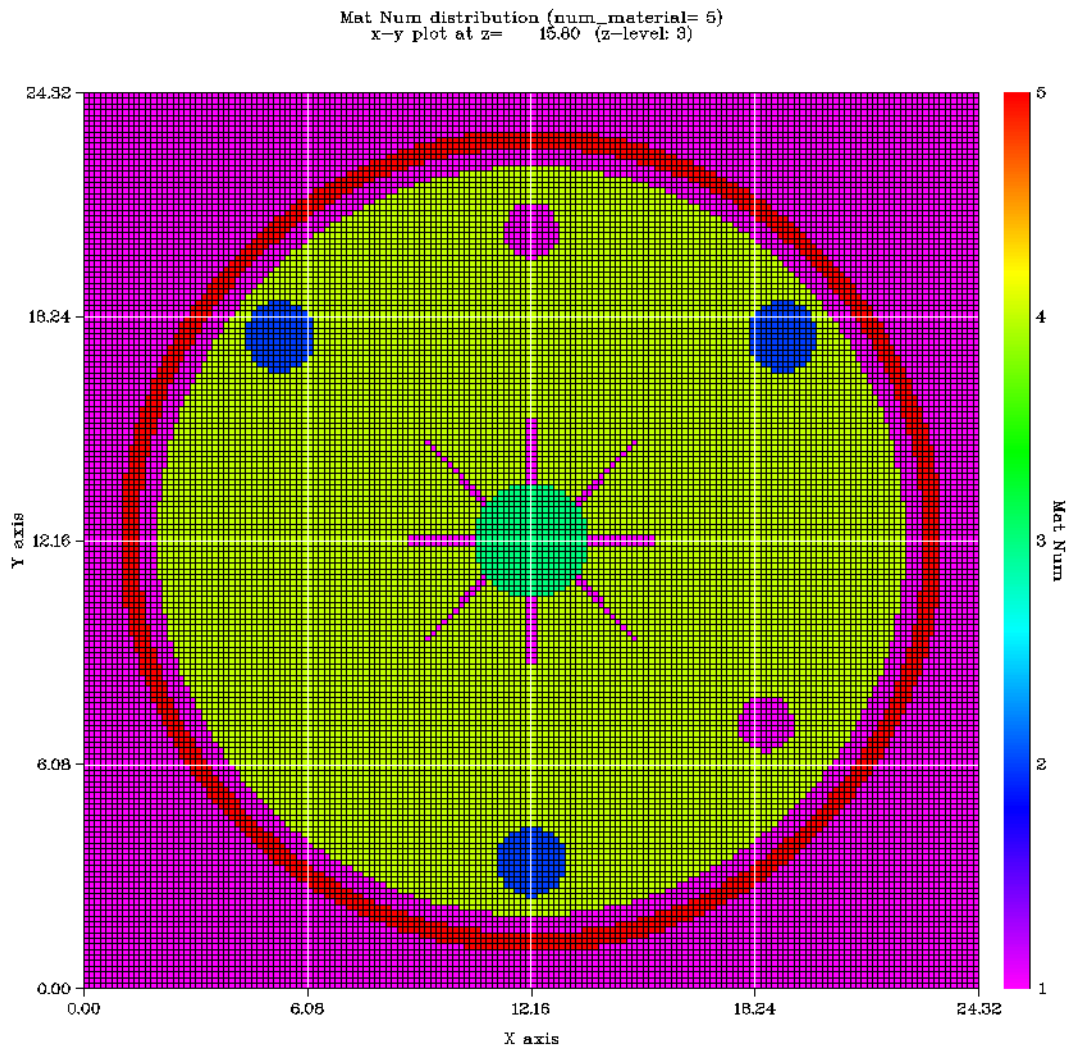


Figure 16. Z-Level Three with Air Flow Grooves

The k_{eff} of the model with air flow grooves was $1.086 \pm 3.4e-4$. The result of this PENTRAN k_{eff} calculation indicates that as more reactor components are modeled which take away fuel, the k_{eff} of the system will be reduced. This “proof of concept” demonstration would be a good starting point for future research to refine the model.

Summary

This chapter discussed the similarities and differences observed between k_{eff} and flux values of different PENTRAN runs as well as an MCNP k_{eff} . Key differences in the PENTRAN runs were examined such as discretization order used (S4, S8), number of energy groups present in the cross-section libraries (10, 47), and Legendre order of the cross-section libraries (P0, P1, P2). Additionally, an analysis of how well the volumes of the constituent model materials were being modeled compared to volume calculations performed outside of PENTRAN was presented. Finally, the investigative questions presented in chapter one of this thesis were examined and answers were presented as a summation of the analysis written before them.

V. Conclusions and Recommendations

Numerous conclusions can be drawn from the results of this research. These conclusions focus primarily on the discretization scheme and Legendre order of the cross-section library used during the various PENTRAN runs. Conclusions can also be drawn regarding the ability of PENTRAN to model a fast burst reactor design.

Based on the parameter studies conducted for this thesis research effort, when using PENTRAN to model the WSMR FBR, there is a maximum difference of 0.003 between the k_{eff} calculated using an S4 or S8 level quadrature schemes if all other parameters are held constant. The suspected reason why the difference between S4 or S8 PENTRAN runs is small when all other parameters are identical is the low amount of scattering occurring in the WSMR FBR due to the energy of the neutrons created during reactor operation. The Legendre order of the cross-section library has a greater affect. When all parameters except the cross-section Legendre order are identical, the maximum k_{eff} difference between two PENTRAN runs is .108. The calculation using the zero order Legendre cross-sections (P0) over predicted the k_{eff} values compared to the PENTRAN runs performed with cross-section libraries using P1 or P2 Legendre order. Because an analogous MCNP model predicted a k_{eff} within a percent relative error to the P1 or P2 PENTRAN runs, it can be concluded that the P1 or P2 PENTRAN runs can represent the range of neutrons generated by the WSMR FBR, while the P0 Legendre order cross-section libraries cannot.

Ultimately, both the MCNP and PENTRAN models are over predicting the k_{eff} of the WSMR FBR in the configuration with the control rods and burst rod removed from

the core. The configuration modeled resulted in a supercritical system despite the fact the configuration should have resulted in a subcritical system [4]. A potential cause for this over prediction of criticality is a greater amount of fuel being present in the model than in the real world WSMR FBR. Additionally, because not all reactor core components were modeled, PENTRAN could be over-calculating the vertical center line flux leading to an increased k_{eff} . These two possibilities are not mutually exclusive and both could be contributing factors. Given the large number of assumptions made regarding dimensions this is not a surprising result.

Significance of Research

This research lays the groundwork for a discrete ordinates code to accurately model a fast burst reactor. Specifically, with model refinement, there is an expectation that PENTRAN will be able to accurately model the FBR. The research also demonstrates the outputs of the discrete ordinates code matched the monte carlo code results. These results lend credibility to PENTRAN's calculations because MCNP is already in use at the WSMR for flux predictions. This research is also likely to impact current WSMR FBR MCNP related research. Specifically, the radiation protection factor work being performed for the Defense Threat Reduction Agency (DTRA). PENTRAN should be able to help future researchers during their design of experiment phase prior to conducting real world tests at the WSMR FBR.

Beyond the direct applications that arise from possessing an accurate flux prediction tool of the WSMR FBR, a series of impacts to other research projects and relationships may be realized. The knowledge that AFIT professors acquired regarding

the running of PENTRAN will allow future AFIT thesis and dissertation projects which incorporate PENTRAN to be performed. This capability will also enable MCNP related projects to be validated against a code which uses a fundamentally different mathematical model from a Monte Carlo code. Also, experimental research efforts can be modeled in PENTRAN in a preliminary fashion to better inform experiments before they are performed.

Recommendations for Future Research

Because the Bugle-96 library was created for thermal reactor modeling and simulation, it is recommended that a cross-section library designed for high energy neutrons is used to identify any significant resultant changes to the k_{eff} or flux predictions. This effort could be accomplished using the Oak Ridge National Lab code NJOY. The primary challenge would be down selecting from a large number of energy groups to choose the optimal set. Additionally, the effects of using higher quadrature level schemes (S16, S32, S50) could be examined to see if significant variations emerge. Finally, the fidelity of the coarse meshes that make up the three dimensional WSMR FBR model could be increased. The last two recommendations would significantly increase the amount of computational resources required, leading to a greater requirement for high performance computing time. As for future PENTRAN model related research, it is recommended that PENTRAN be used on all AFIT research projects requiring flux or k_{eff} calculations to be performed.

It is also recommended that future work attempts to identify exact WSMR FBR dimensions so that the k_{eff} of the model in the configuration created for this research

effort is reduced to subcritical. k_{eff} could also be reduced by replacing areas of the model which currently contain fuel with the proper material. This could be done by adding in reactor details left out of such as the vent holes, air flow grooves, and thermocouple hole. Modeling additional reactor details would remove fuel and should lower the system k_{eff} .

Appendix A. PENMSHXP/PENTRAN Input Files

PENMSH.INP File:

```
ceres
/no. coarse z-levels, no. of materials, imath
6,5,0
/z-level coarse mesh boundaries
0.0,1.27,14.19606,17.4117,20.32,20.955,22.225
/max. number of fine z-mesh per coarse z-level
100 100 100 100 100 100
/fine-to-med grid ratio along x.., y.., z.. in each coarse z-level
2 2 2 2 2
2 2 2 2 2
2 2 2 2 2
/source format iso, # x-src mesh, # y-src mesh, # z-src mesh, ngrp, sn, pn
2,1,1,1,10,4,0
/xsec type, xsec #comment cards, xsec Leg order, ihm
1, 1, 0, 13
/Bdy conds: ibback(-x),ibfrnt(+x),jbeast(-y),jbwest(+y),kbsout(-z),kbnort(+z)
0,0,0,0,0,0
```

CERES1.INP File

```
/ncx, ncy, maxfinz (maxfinz < 1, add z-fine per cm below y-fine)
4,4,-1
/ x-fine mesh per cm (# seq along cm rows of x)
30 30 30 30
30 30 30 30
30 30 30 30
30 30 30 30
/ y-fine mesh per cm (# seq ... x)
30 30 30 30
30 30 30 30
30 30 30 30
30 30 30 30
/ z-fine mesh per cm (# seq ... x)
4 4 4 4
4 4 4 4
4 4 4 4
4 4 4 4
/ cm bounds along x-axis (in seq ...x)
0.0,6.0795,12.159,18.2385,24.318
```

```
/cm bounds along y-axis (in seq ...y)
0.0,6.0795,12.159,18.2385,24.318
/ cm type, each cm (<0 =look for overlay)
-1 -1 -1 -1
-1 -1 -1 -1
-1 -1 -1 -1
-1 -1 -1 -1
/ number of material regions per coarse mesh
1 1 1 1
1 1 1 1
1 1 1 1
1 1 1 1
/ coarse mesh 1
1
/ coarse mesh 2
1
/ coarse mesh 3
1
/ coarse mesh 4
1
/ coarse mesh 5
1
/ coarse mesh 6
1
/ coarse mesh 7
1
/ coarse mesh 8
1
/ coarse mesh 9
1
/ coarse mesh 10
1
/ coarse mesh 11
1
/ coarse mesh 12
1
/ coarse mesh 13
1
/ coarse mesh 14
1
/ coarse mesh 15
1
/ coarse mesh 16
1
```

```
/overlay cm 1
1
2
3
0.5 23.82 0.5 23.82
/overlay cm 2
1
2
3
0.5 23.82 0.5 23.82
/overlay cm 3
1
2
3
0.5 23.82 0.5 23.82
/overlay cm 4
1
2
3
0.5 23.82 0.5 23.82
/overlay cm 5
1
2
3
0.5 23.82 0.5 23.82
/overlay cm 6
1
2
3
0.5 23.82 0.5 23.82
/overlay cm 7
1
2
3
0.5 23.82 0.5 23.82
/overlay cm 8
1
2
3
0.5 23.82 0.5 23.82
/overlay cm 9
1
2
3
0.5 23.82 0.5 23.82
```



```
/overlay cm 10
1
2
3
0.5 23.82 0.5 23.82
/overlay cm 11
1
2
3
0.5 23.82 0.5 23.82
/overlay cm 12
1
2
3
0.5 23.82 0.5 23.82
/overlay cm 13
1
2
3
0.5 23.82 0.5 23.82
/overlay cm 14
1
2
3
0.5 23.82 0.5 23.82
/overlay cm 15
1
2
3
0.5 23.82 0.5 23.82
/overlay cm 16
1
2
3
0.5 23.82 0.5 23.82
/overlay cm 1: boron loaded silicate shroud
/7
/2 2 2 2 2 2
/5 1 4 2 2 2 3
/1 23.32 1 23.32
/1.5 22.82 1.5 22.82
/2 22.32 2 22.32
/11.2075 13.1125 2.5 4.405
/18.0375 19.9425 16.75 18.655
/4.3775 6.2825 16.75 18.655
```

CERES2.INP File

```
/ncx, ncy, maxfinz (maxfinz < 0, add z-fine per cm below y-fine)
4,4,-1
/ x-fine mesh per cm (# seq along cm rows of x)
30 30 30 30
30 30 30 30
30 30 30 30
30 30 30 30
/ y-fine mesh per cm (# seq ... x)
30 30 30 30
30 30 30 30
30 30 30 30
30 30 30 30
/ z-fine mesh per cm (# seq ... x)
30 30 30 30
30 30 30 30
30 30 30 30
30 30 30 30
/ cm bounds along x-axis (in seq ...x)
0.0,6.0795,12.159,18.2385,24.318
/cm bounds along y-axis (in seq ...x)
0.0,6.0795,12.159,18.2385,24.318
/ cm type, each cm (<0 =look for overlay)
-1 -1 -1 -1
-1 -1 -1 -1
-1 -1 -1 -1
-1 -1 -1 -1
/ number of material regions per coarse mesh
1 1 1 1
1 1 1 1
1 1 1 1
1 1 1 1
/ coarse mesh 1
1
/ coarse mesh 2
1
/ coarse mesh 3
1
/ coarse mesh 4
1
/ coarse mesh 5
1
```

```
/ coarse mesh 6
1
/ coarse mesh 7
1
/ coarse mesh 8
1
/ coarse mesh 9
1
/ coarse mesh 10
1
/ coarse mesh 11
1
/ coarse mesh 12
1
/ coarse mesh 13
1
/ coarse mesh 14
1
/ coarse mesh 15
1
/ coarse mesh 16
1
/overlay cm 1
3
2 2 2
5 1 4
1 23.32 1 23.32
1.5 22.82 1.5 22.82
2 22.32 2 22.32
/overlay cm 2
4
2 2 2 2
5 1 4 2
1 23.32 1 23.32
1.5 22.82 1.5 22.82
2 22.32 2 22.32
11.2075 13.1125 2.5 4.405
/overlay cm 3
4
2 2 2 2
5 1 4 2
1 23.32 1 23.32
1.5 22.82 1.5 22.82
2 22.32 2 22.32
11.2075 13.1125 2.5 4.405
```

```
/overlay cm 4
3
2 2 2
5 1 4
1 23.32 1 23.32
1.5 22.82 1.5 22.82
2 22.32 2 22.32
/overlay cm 5
4
2 2 2 2
5 1 4 1
1 23.32 1 23.32
1.5 22.82 1.5 22.82
2 22.32 2 22.32
5.03 6.53 6.45 7.95
/overlay cm 6
5
2 2 2 2 2
5 1 4 3 1
1 23.32 1 23.32
1.5 22.82 1.5 22.82
2 22.32 2 22.32
10.5725 13.7475 10.5725 13.7475
5.03 6.53 6.45 7.95
/overlay cm 7
5
2 2 2 2 2
5 1 4 3 1
1 23.32 1 23.32
1.5 22.82 1.5 22.82
2 22.32 2 22.32
10.5725 13.7475 10.5725 13.7475
17.79 19.29 6.45 7.95
/overlay cm 8
4
2 2 2 2
5 1 4 1
1 23.32 1 23.32
1.5 22.82 1.5 22.82
2 22.32 2 22.32
17.79 19.29 6.45 7.95
```

```
/overlay cm 9
4
2 2 2 2
5 1 4 2
1 23.32 1 23.32
1.5 22.82 1.5 22.82
2 22.32 2 22.32
4.3775 6.2825 16.75 18.655
/overlay cm 10
5
2 2 2 2 2
5 1 4 3 2
1 23.32 1 23.32
1.5 22.82 1.5 22.82
2 22.32 2 22.32
10.5725 13.7475 10.5725 13.7475
4.3775 6.2825 16.75 18.655
/overlay cm 11
5
2 2 2 2 2
5 1 4 3 2
1 23.32 1 23.32
1.5 22.82 1.5 22.82
2 22.32 2 22.32
10.5725 13.7475 10.5725 13.7475
18.0375 19.9425 16.75 18.655
/overlay cm 12
4
2 2 2 2
5 1 4 2
1 23.32 1 23.32
1.5 22.82 1.5 22.82
2 22.32 2 22.32
18.0375 19.9425 16.75 18.655
/overlay cm 13
4
2 2 2 2
5 1 4 2
1 23.32 1 23.32
1.5 22.82 1.5 22.82
2 22.32 2 22.32
4.3775 6.2825 16.75 18.655
```

```
/overlay cm 14
5
2 2 2 2
5 1 4 2 1
1 23.32 1 23.32
1.5 22.82 1.5 22.82
2 22.32 2 22.32
4.3775 6.2825 16.75 18.655
11.41 12.91 19.82 21.32
/overlay cm 15
5
2 2 2 2
5 1 4 2 1
1 23.32 1 23.32
1.5 22.82 1.5 22.82
2 22.32 2 22.32
18.0375 19.9425 16.75 18.655
11.41 12.91 19.82 21.32
/overlay cm 16
4
2 2 2 2
5 1 4 2
1 23.32 1 23.32
1.5 22.82 1.5 22.82
2 22.32 2 22.32
18.0375 19.9425 16.75 18.655
/overlay cm 1: boron loaded silicate shroud
/7
/2 2 2 2 2 2
/5 1 4 2 2 2 3
/1 23.32 1 23.32
/1.5 22.82 1.5 22.82
/2 22.32 2 22.32
/11.2075 13.1125 2.5 4.405
/18.0375 19.9425 16.75 18.655
/4.3775 6.2825 16.75 18.655
/10.5725 13.7475 10.5725 13.7475
```

CERES3.INP File

```
/ncx, ncy, maxfinz (maxfinz < 0, add z-fine per cm below y-fine)
4,4,-1
/ x-fine mesh per cm (# seq along cm rows of x)
30 30 30 30
30 30 30 30
30 30 30 30
30 30 30 30
/ y-fine mesh per cm (# seq ... x)
30 30 30 30
30 30 30 30
30 30 30 30
30 30 30 30
/ z-fine mesh per cm (# seq ... x)
7 7 7 7
7 7 7 7
7 7 7 7
7 7 7 7
/ cm bounds along x-axis (in seq ...x)
0.0,6.0795,12.159,18.2385,24.318
/cm bounds along y-axis (in seq ...x)
0.0,6.0795,12.159,18.2385,24.318
/ cm type, each cm (<0 =look for overlay)
-1 -1 -1 -1
-1 -1 -1 -1
-1 -1 -1 -1
-1 -1 -1 -1
/ number of material regions per coarse mesh
1 1 1 1
1 1 1 1
1 1 1 1
1 1 1 1
/ coarse mesh 1
1
/ coarse mesh 2
1
/ coarse mesh 3
1
/ coarse mesh 4
1
/ coarse mesh 5
1
```

```

/coarse mesh 6
1
/coarse mesh 7
1
/coarse mesh 8
1
/coarse mesh 9
1
/coarse mesh 10
1
/coarse mesh 11
1
/coarse mesh 12
1
/coarse mesh 13
1
/coarse mesh 14
1
/coarse mesh 15
1
/coarse mesh 16
1
/overlay cm 1
3
2 2 2
5 1 4
1 23.32 1 23.32
1.5 22.82 1.5 22.82
2 22.32 2 22.32
/overlay cm 2
4
2 2 2 2
5 1 4 2
1 23.32 1 23.32
1.5 22.82 1.5 22.82
2 22.32 2 22.32
11.2075 13.1125 2.5 4.405
/overlay cm 3
4
2 2 2 2
5 1 4 2
1 23.32 1 23.32
1.5 22.82 1.5 22.82
2 22.32 2 22.32
11.2075 13.1125 2.5 4.405

```



```
/overlay cm 4
3
2 2 2
5 1 4
1 23.32 1 23.32
1.5 22.82 1.5 22.82
2 22.32 2 22.32
/overlay cm 5
3
2 2 2
5 1 4
1 23.32 1 23.32
1.5 22.82 1.5 22.82
2 22.32 2 22.32
/overlay cm 6
4
2 2 2 2
5 1 4 3
1 23.32 1 23.32
1.5 22.82 1.5 22.82
2 22.32 2 22.32
10.5725 13.7475 10.5725 13.7475
/overlay cm 7
5
2 2 2 2 2
5 1 4 3 1
1 23.32 1 23.32
1.5 22.82 1.5 22.82
2 22.32 2 22.32
10.5725 13.7475 10.5725 13.7475
17.79 19.29 6.45 7.95
/overlay cm 8
4
2 2 2 2
5 1 4 1
1 23.32 1 23.32
1.5 22.82 1.5 22.82
2 22.32 2 22.32
17.79 19.29 6.45 7.95
```

```
/overlay cm 9
4
2 2 2 2
5 1 4 2
1 23.32 1 23.32
1.5 22.82 1.5 22.82
2 22.32 2 22.32
4.3775 6.2825 16.75 18.655
/overlay cm 10
5
2 2 2 2 2
5 1 4 3 2
1 23.32 1 23.32
1.5 22.82 1.5 22.82
2 22.32 2 22.32
10.5725 13.7475 10.5725 13.7475
4.3775 6.2825 16.75 18.655
/overlay cm 11
5
2 2 2 2 2
5 1 4 3 2
1 23.32 1 23.32
1.5 22.82 1.5 22.82
2 22.32 2 22.32
10.5725 13.7475 10.5725 13.7475
18.0375 19.9425 16.75 18.655
/overlay cm 12
4
2 2 2 2
5 1 4 2
1 23.32 1 23.32
1.5 22.82 1.5 22.82
2 22.32 2 22.32
18.0375 19.9425 16.75 18.65
/overlay cm 13
4
2 2 2 2
5 1 4 2
1 23.32 1 23.32
1.5 22.82 1.5 22.82
2 22.32 2 22.32
4.3775 6.2825 16.75 18.655
```

```
/overlay cm 14
5
2 2 2 2 2
5 1 4 2 1
1 23.32 1 23.32
1.5 22.82 1.5 22.82
2 22.32 2 22.32
4.3775 6.2825 16.75 18.655
11.41 12.91 19.82 21.32
/overlay cm 15
5
2 2 2 2 2
5 1 4 2 1
1 23.32 1 23.32
1.5 22.82 1.5 22.82
2 22.32 2 22.32
18.0375 19.9425 16.75 18.655
11.41 12.91 19.82 21.32
/overlay cm 16
4
2 2 2 2
5 1 4 2
1 23.32 1 23.32
1.5 22.82 1.5 22.82
2 22.32 2 22.32
18.0375 19.9425 16.75 18.655
/overlay cm 1: boron loaded silicate shroud
/7
/2 2 2 2 2 2 2
/5 1 4 2 2 2 3
/1 23.32 1 23.32
/1.5 22.82 1.5 22.82
/2 22.32 2 22.32
/11.2075 13.1125 2.5 4.405
/18.0375 19.9425 16.75 18.655
/4.3775 6.2825 16.75 18.655
/10.5725 13.7475 10.5725 13.7475
```

CERES4.INP File

```
/ncx, ncy, maxfinz (maxfinz < 0, add z-fine per cm below y-fine)
4,4,-1
/x-fine mesh per cm (# seq along cm rows of x)
30 30 30 30
30 30 30 30
30 30 30 30
30 30 30 30
/y-fine mesh per cm (# seq ... x)
30 30 30 30
30 30 30 30
30 30 30 30
/z-fine mesh per cm (# seq ... x)
7 7 7 7
7 7 7 7
7 7 7 7
7 7 7 7
/cm bounds along x-axis (in seq ...x)
0.0,6.0795,12.159,18.2385,24.318
/cm bounds along y-axis (in seq ...x)
0.0,6.0795,12.159,18.2385,24.318
/cm type, each cm (<0 =look for overlay)
-1 -1 -1 -1
-1 -1 -1 -1
-1 -1 -1 -1
-1 -1 -1 -1
/ number of material regions per coarse mesh
1 1 1 1
1 1 1 1
1 1 1 1
1 1 1 1
/coarse mesh 1
1
/coarse mesh 2
1
/coarse mesh 3
1
/coarse mesh 4
1
/coarse mesh 5
1
```

```

/coarse mesh 6
1
/coarse mesh 7
1
/coarse mesh 8
1
/coarse mesh 9
1
/coarse mesh 10
1
/coarse mesh 11
1
/coarse mesh 12
1
/coarse mesh 13
1
/coarse mesh 14
1
/coarse mesh 15
1
/coarse mesh 16
1
/overlay cm 1
3
2 2 2
5 1 4
1 23.32 1 23.32
1.5 22.82 1.5 22.82
2 22.32 2 22.32
/overlay cm 2
4
2 2 2 2
5 1 4 2
1 23.32 1 23.32
1.5 22.82 1.5 22.82
2 22.32 2 22.32
11.2075 13.1125 2.5 4.405
/overlay cm 3
4
2 2 2 2
5 1 4 2
1 23.32 1 23.32
1.5 22.82 1.5 22.82
2 22.32 2 22.32
11.2075 13.1125 2.5 4.405

```

```
/overlay cm 4
3
2 2 2
5 1 4
1 23.32 1 23.32
1.5 22.82 1.5 22.82
2 22.32 2 22.32
/overlay cm 5
3
2 2 2
5 1 4
1 23.32 1 23.32
1.5 22.82 1.5 22.82
2 22.32 2 22.32
/overlay cm 6
5
2 2 2 2 2
5 1 4 3 3
1 23.32 1 23.32
1.5 22.82 1.5 22.82
2 22.32 2 22.32
10.5725 13.7475 10.5725 13.7475
8.349 15.969 8.349 15.969
/overlay cm 7
5
2 2 2 2 2
5 1 4 3 3
1 23.32 1 23.32
1.5 22.82 1.5 22.82
2 22.32 2 22.32
10.5725 13.7475 10.5725 13.7475
8.349 15.969 8.349 15.969
/overlay cm 8
3
2 2 2
5 1 4
1 23.32 1 23.32
1.5 22.82 1.5 22.82
2 22.32 2 22.32
```

/overlay cm 9
4
2 2 2 2
5 1 4 2
1 23.32 1 23.32
1.5 22.82 1.5 22.82
2 22.32 2 22.32
4.3775 6.2825 16.75 18.655
/overlay cm 10
6
2 2 2 2 2 2
5 1 4 3 2 3
1 23.32 1 23.32
1.5 22.82 1.5 22.82
2 22.32 2 22.32
10.5725 13.7475 10.5725 13.7475
4.3775 6.2825 16.75 18.655
8.349 15.969 8.349 15.969
/overlay cm 11
6
2 2 2 2 2 2
5 1 4 3 2 3
1 23.32 1 23.32
1.5 22.82 1.5 22.82
2 22.32 2 22.32
10.5725 13.7475 10.5725 13.7475
18.0375 19.9425 16.75 18.655
8.349 15.969 8.349 15.969
/overlay cm 12
4
2 2 2 2
5 1 4 2
1 23.32 1 23.32
1.5 22.82 1.5 22.82
2 22.32 2 22.32
18.0375 19.9425 16.75 18.655
/overlay cm 13
4
2 2 2 2
5 1 4 2
1 23.32 1 23.32
1.5 22.82 1.5 22.82
2 22.32 2 22.32
4.3775 6.2825 16.75 18.655

```
/overlay cm 14
4
2 2 2 2
5 1 4 2
1 23.32 1 23.32
1.5 22.82 1.5 22.82
2 22.32 2 22.32
4.3775 6.2825 16.75 18.655
/overlay cm 15
4
2 2 2 2
5 1 4 2
1 23.32 1 23.32
1.5 22.82 1.5 22.82
2 22.32 2 22.32
18.0375 19.9425 16.75 18.655
/overlay cm 16
4
2 2 2 2
5 1 4 2
1 23.32 1 23.32
1.5 22.82 1.5 22.82
2 22.32 2 22.32
18.0375 19.9425 16.75 18.655
/overlay cm 1: boron loaded silicate shroud
/7
/2 2 2 2 2 2
/5 1 4 2 2 2 3
/1 23.32 1 23.32
/1.5 22.82 1.5 22.82
/2 22.32 2 22.32
/11.2075 13.1125 2.5 4.405
/18.0375 19.9425 16.75 18.655
/4.3775 6.2825 16.75 18.655
/10.5725 13.7475 10.5725 13.7475
```


CERES5.INP File

```
/ncx, ncy, maxfinz (maxfinz < 0, add z-fine per cm below y-fine)
4,4,-1
/x-fine mesh per cm (# seq along cm rows of x)
30 30 30 30
30 30 30 30
30 30 30 30
30 30 30 30
/y-fine mesh per cm (# seq ... x)
30 30 30 30
30 30 30 30
30 30 30 30
/z-fine mesh per cm (# seq ... x)
2 2 2 2
2 2 2 2
2 2 2 2
/cm bounds along x-axis (in seq ...x)
0.0,6.0795,12.159,18.2385,24.318
/cm bounds along y-axis (in seq ...x)
0.0,6.0795,12.159,18.2385,24.318
/cm type, each cm (<0 =look for overlay)
-1 -1 -1 -1
-1 -1 -1 -1
-1 -1 -1 -1
-1 -1 -1 -1
/ number of material regions per coarse mesh
1 1 1 1
1 1 1 1
1 1 1 1
1 1 1 1
/coarse mesh 1
1
/coarse mesh 2
1
/coarse mesh 3
1
/coarse mesh 4
1
/coarse mesh 5
1
```

```
/ coarse mesh 6
1
/ coarse mesh 7
1
/ coarse mesh 8
1
/ coarse mesh 9
1
/ coarse mesh 10
1
/ coarse mesh 11
1
/ coarse mesh 12
1
/ coarse mesh 13
1
/ coarse mesh 14
1
/ coarse mesh 15
1
/ coarse mesh 16
1
/overlay cm 1
2
2 2
5 1
1 23.32 1 23.32
1.5 22.82 1.5 22.82
/overlay cm 2
3
2 2 2
5 1 2
1 23.32 1 23.32
1.5 22.82 1.5 22.82
11.2075 13.1125 2.5 4.405
/overlay cm 3
3
2 2 2
5 1 2
1 23.32 1 23.32
1.5 22.82 1.5 22.82
11.2075 13.1125 2.5 4.405
```

```
/overlay cm 4
2
2 2
5 1
1 23.32 1 23.32
1.5 22.82 1.5 22.82
/overlay cm 5
2
2 2
5 1
1 23.32 1 23.32
1.5 22.82 1.5 22.82
/overlay cm 6
2
2 2
5 1
1 23.32 1 23.32
1.5 22.82 1.5 22.82
/overlay cm 7
2
2 2
5 1
1 23.32 1 23.32
1.5 22.82 1.5 22.82
/overlay cm 8
2
2 2
5 1
1 23.32 1 23.32
1.5 22.82 1.5 22.82
/overlay cm 9
3
2 2 2
5 1 2
1 23.32 1 23.32
1.5 22.82 1.5 22.82
4.3775 6.2825 16.75 18.655
```

```
/overlay cm 10
3
2 2 2
5 1 2
1 23.32 1 23.32
1.5 22.82 1.5 22.82
4.3775 6.2825 16.75 18.655
/overlay cm 11
3
2 2 2
5 1 2
1 23.32 1 23.32
1.5 22.82 1.5 22.82
18.0375 19.9425 16.75 18.655
/overlay cm 12
3
2 2 2
5 1 2
1 23.32 1 23.32
1.5 22.82 1.5 22.82
18.0375 19.9425 16.75 18.655
/overlay cm 13
3
2 2 2
5 1 2
1 23.32 1 23.32
1.5 22.82 1.5 22.82
4.3775 6.2825 16.75 18.655
/overlay cm 14
3
2 2 2
5 1 2
1 23.32 1 23.32
1.5 22.82 1.5 22.82
4.3775 6.2825 16.75 18.655
/overlay cm 15
3
2 2 2
5 1 2
1 23.32 1 23.32
1.5 22.82 1.5 22.82
18.0375 19.9425 16.75 18.655
```

```

/overlay cm 16
3
2 2 2
5 1 2
1 23.32 1 23.32
1.5 22.82 1.5 22.82
18.0375 19.9425 16.75 18.655
/overlay cm 1: boron loaded silicate shroud
/7
/2 2 2 2 2 2
/5 1 4 2 2 2 3
/1 23.32 1 23.32
/1.5 22.82 1.5 22.82
/2 22.32 2 22.32
/11.2075 13.1125 2.5 4.405
/18.0375 19.9425 16.75 18.655
/4.3775 6.2825 16.75 18.655
/10.5725 13.7475 10.5725 13.7475

```

CERES6.INP File

```

/ncx, ncy, maxfinz (maxfinz < 0, add z-fine per cm below y-fine)
4,4,-1
/ x-fine mesh per cm (# seq along cm rows of x)
30 30 30 30
30 30 30 30
30 30 30 30
30 30 30 30
/ y-fine mesh per cm (# seq ... x)
30 30 30 30
30 30 30 30
30 30 30 30
30 30 30 30
/ z-fine mesh per cm (# seq ... x)
3 3 3 3
3 3 3 3
3 3 3 3
3 3 3 3

```

```

/cm bounds along x-axis (in seq ...x)
0.0,6.0795,12.159,18.2385,24.318
/cm bounds along y-axis (in seq ...x)
0.0,6.0795,12.159,18.2385,24.318
/cm type, each cm (<0 =look for overlay)
-1 -1 -1 -1
-1 -1 -1 -1
-1 -1 -1 -1
-1 -1 -1 -1
/cm number of material regions per coarse mesh
1 1 1 1
1 1 1 1
1 1 1 1
1 1 1 1
/cm coarse mesh 1
1
/cm coarse mesh 2
1
/cm coarse mesh 3
1
/cm coarse mesh 4
1
/cm coarse mesh 5
1
/cm coarse mesh 6
1
/cm coarse mesh 7
1
/cm coarse mesh 8
1
/cm coarse mesh 9
1
/cm coarse mesh 10
1
/cm coarse mesh 11
1
/cm coarse mesh 12
1
/cm coarse mesh 13
1
/cm coarse mesh 14
1
/cm coarse mesh 15
1

```

```
/ coarse mesh 16
1
/overlay cm 1
1
2
5
1 23.32 1 23.32
/overlay cm 2
1
2
5
1 23.32 1 23.32
/overlay cm 3
1
2
5
1 23.32 1 23.32
/overlay cm 4
1
2
5
1 23.32 1 23.32
/overlay cm 5
1
2
5
1 23.32 1 23.32
/overlay cm 6
1
2
5
1 23.32 1 23.32
/overlay cm 7
1
2
5
1 23.32 1 23.32
/overlay cm 8
1
2
5
1 23.32 1 23.32
```

```
/overlay cm 9
1
2
5
1 23.32 1 23.32
/overlay cm 10
1
2
5
1 23.32 1 23.32
/overlay cm 11
1
2
5
1 23.32 1 23.32
/overlay cm 12
1
2
5
1 23.32 1 23.32
/overlay cm 13
1
2
5
1 23.32 1 23.32
/overlay cm 14
1
2
5
1 23.32 1 23.32
/overlay cm 15
1
2
5
1 23.32 1 23.32
/overlay cm 16
1
2
5
1 23.32 1 23.32
```



```

/overlay cm 1: boron loaded silicate shroud
/7
/2 2 2 2 2 2
/5 1 4 2 2 2 3
/1 23.32 1 23.32
/1.5 22.82 1.5 22.82
/2 22.32 2 22.32
/11.2075 13.1125 2.5 4.405
/18.0375 19.9425 16.75 18.655
/4.3775 6.2825 16.75 18.655
/10.5725 13.7475 10.5725 13.7475

```

CERES.PEN (S4 P0 47 Group Run)

```

PARAMETERS FOR MEMORY ALLOCATION :
maxmem, maxpcs, maxgcm, maxxsg
4096      16      96      47
maxcmc, maxcrs, maxmmc, maxmed, maxfmc, maxfin
96        6      1600    40      1600    40
maxgrp, maxglc, maxswp, maxqdm, maxmat, maxleg
47        47      8        3        5        0
maxsrc, maxslc, maxcmr, maxlin, maxarr, nctlim
0         0       96      860    354300 3380
/-----Start Problem Deck-----
ceres                                loglevel 2
generated by PENMSHXP version 2.74b (08.10.2014)
Total Number of Fine Meshes: 153600
Total Number of Coarse Meshes: 96
Number of zlevs: 6
Number of coarse mesh per z lev: 16
6
7
8
9
10
/

```

```

/-----BLOCK I (GENERAL PROBLEM info.)-----
/
ngeom=3d
modadj=0
ngroup=47
isn=4
nmatl=5
ixcrs=4
jycrs=4
kzcrs=6
lodbal=0
timcut=0.
tolmgd=-0.200
decmpv=8 1 2 T
/
/-----BLOCK II(geometry)-----
/
/ x coarse-mesh position
/
xmesh= 0.0000E+00 6.0795E+00 1.2159E+01 1.8239E+01 2.4318E+01
/
/ x fine mesh distribution for zlev= 1
/
ixfine=40 40 40 40
      40 40 40 40
      40 40 40 40
      40 40 40 40
/
/ x fine mesh distribution for zlev= 2
/
      40 40 40 40
      40 40 40 40
      40 40 40 40
      40 40 40 40
/
/ x fine mesh distribution for zlev= 3
/
      40 40 40 40
      40 40 40 40
      40 40 40 40
      40 40 40 40
/

```

```
/ x fine mesh distribution for zlev= 4
/
  40 40 40 40
  40 40 40 40
  40 40 40 40
  40 40 40 40
/
/ x fine mesh distribution for zlev= 5
/
  40 40 40 40
  40 40 40 40
  40 40 40 40
  40 40 40 40
/
/ x fine mesh distribution for zlev= 6
/
  40 40 40 40
  40 40 40 40
  40 40 40 40
  40 40 40 40
/
/ x medium mesh distribution for zlev= 1
/
ixmed=20 20 20 20
  20 20 20 20
  20 20 20 20
  20 20 20 20
/
/ x medium mesh distribution for zlev= 2
/
  20 20 20 20
  20 20 20 20
  20 20 20 20
  20 20 20 20
/
/ x medium mesh distribution for zlev= 3
/
  20 20 20 20
  20 20 20 20
  20 20 20 20
  20 20 20 20
```

```
/
/x medium mesh distribution for zlev= 4
/
 20 20 20 20
 20 20 20 20
 20 20 20 20
 20 20 20 20
/
/x medium mesh distribution for zlev= 5
/
 20 20 20 20
 20 20 20 20
 20 20 20 20
 20 20 20 20
/
/x medium mesh distribution for zlev= 6
/
 20 20 20 20
 20 20 20 20
 20 20 20 20
 20 20 20 20
/
/y coarse-mesh position
/
ymesh= 0.0000E+00 6.0795E+00 1.2159E+01 1.8239E+01 2.4318E+01
/
/y fine mesh distribution for zlev= 1
/
jyfine=40 40 40 40
 40 40 40 40
 40 40 40 40
 40 40 40 40
/
/y fine mesh distribution for zlev= 2
/
 40 40 40 40
 40 40 40 40
 40 40 40 40
 40 40 40 40
/
```

```
/ y fine mesh distribution for zlev= 3
/
40 40 40 40
40 40 40 40
40 40 40 40
40 40 40 40
/
/ y fine mesh distribution for zlev= 4
/
40 40 40 40
40 40 40 40
40 40 40 40
40 40 40 40
/
/ y fine mesh distribution for zlev= 5
/
40 40 40 40
40 40 40 40
40 40 40 40
40 40 40 40
/
/ y fine mesh distribution for zlev= 6
/
40 40 40 40
40 40 40 40
40 40 40 40
40 40 40 40
/
/ y medium mesh distribution for zlev= 1
/
jymed=20 20 20 20
20 20 20 20
20 20 20 20
20 20 20 20
/
/ y medium mesh distribution for zlev= 2
/
20 20 20 20
20 20 20 20
20 20 20 20
20 20 20 20
/
```

```

/y medium mesh distribution for zlev= 3
/
20 20 20 20
20 20 20 20
20 20 20 20
20 20 20 20
/
/y medium mesh distribution for zlev= 4
/
20 20 20 20
20 20 20 20
20 20 20 20
20 20 20 20
/
/y medium mesh distribution for zlev= 5
/
20 20 20 20
20 20 20 20
20 20 20 20
20 20 20 20
/
/y medium mesh distribution for zlev= 6
/
20 20 20 20
20 20 20 20
20 20 20 20
20 20 20 20
/
/z coarse-mesh position
/
zmesh= 0.0000E+00 1.2700E+00 1.4196E+01 1.7412E+01 2.0320E+01
2.0955E+01 2.2225E+01
/
/z fine mesh distribution for zlev= 1
/
kzfine=1 1 1 1
1 1 1 1
1 1 1 1
1 1 1 1

```

```
/
/z fine mesh distribution for zlev= 2
/
  1 1 1 1
  1 1 1 1
  1 1 1 1
  1 1 1 1
/
/z fine mesh distribution for zlev= 3
/
  1 1 1 1
  1 1 1 1
  1 1 1 1
  1 1 1 1
/
/z fine mesh distribution for zlev= 4
/
  1 1 1 1
  1 1 1 1
  1 1 1 1
  1 1 1 1
/
/z fine mesh distribution for zlev= 5
/
  1 1 1 1
  1 1 1 1
  1 1 1 1
  1 1 1 1
/
/z fine mesh distribution for zlev= 6
/
  1 1 1 1
  1 1 1 1
  1 1 1 1
  1 1 1 1
/
/z medium mesh distribution for zlev= 1
/
kzmed=1 1 1 1
  1 1 1 1
  1 1 1 1
  1 1 1 1
```

```

/
/z medium mesh distribution for zlev= 2
/
  1 1 1 1
  1 1 1 1
  1 1 1 1
  1 1 1 1
/
/z medium mesh distribution for zlev= 3
/
  1 1 1 1
  1 1 1 1
  1 1 1 1
  1 1 1 1
/
/z medium mesh distribution for zlev= 4
/
  1 1 1 1
  1 1 1 1
  1 1 1 1
  1 1 1 1
/
/z medium mesh distribution for zlev= 5
/
  1 1 1 1
  1 1 1 1
  1 1 1 1
  1 1 1 1
/
/z medium mesh distribution for zlev= 6
/
  1 1 1 1
  1 1 1 1
  1 1 1 1
  1 1 1 1
/
/ material distribution for zlev= 1
/
  nmattp=1
638R1 2R3 37R1 3R3 36R1 4R3 34R1 6R3 33R1 7R3 32R1 8R3 30R1 10R3 29R1
11R3
28R1 12R3 27R1 13R3 26R1 14R3 25R1 15R3 24R1 16R3 23R1 17R3 22R1 18R3
21R1
19R3 1Q40 20R1 20R3 19R1 21R3 18R1 22R3 1Q40 17R1 23R3 16R1 24R3 15R1
25R3

```


nmattp=2
 154R1 6R3 26R1 14R3 22R1 18R3 18R1 22R3 15R1 25R3 12R1 28R3 10R1 30R3
 8R1 32R3
 5R1 35R3 4R1 36R3 2R1 1078R3
 nmattp=3
 120R1 6R3 1Q40 8R3 1Q40 4R3 1Q40 4R3 1Q40 3R3 1Q40 3R3 1Q40 2R3 1Q40
 2R3 1Q40
 3R3 1Q40 3 1Q40 2R3 1Q40 1002R3
 nmattp=4
 600R1 2R3 1Q40 3 1Q40 3 1Q40 2R3 1Q40 3 1Q40 3 1Q40 2R3 1Q40 3 1Q40 3
 1Q40 3
 1Q40 3 1Q40 3 1Q40 3 1Q40 3 1Q40 3 1Q40 3 2Q40 3 1Q40 3 1Q40 3 2Q40 3 1Q40
 3
 1Q40 3 1Q40 15R1
 nmattp=5
 14R1 26R3 1Q40 13R1 27R3 1Q40 12R1 28R3 11R1 29R3 2Q40 10R1 30R3 1Q40
 9R1 31R3
 1Q40 8R1 32R3 2Q40 7R1 33R3 2Q40 6R1 34R3 3Q40 5R1 35R3 3Q40 4R1 36R3
 7Q40 3R1
 37R3 5Q40
 nmattp=6
 1600R3
 nmattp=7
 1600R3
 nmattp=8
 26R3 14R1 1Q40 27R3 2Q40 3 1Q40 3 3Q40 3 2Q40 3 2Q40 3 3Q40 3 3Q40 3 4Q40
 3
 4Q40 3 8Q40 3 5Q40 3R1
 nmattp=9
 3R1 37R3 5Q40 4R1 8Q40 1 4Q40 1 4Q40 1 3Q40 1 3Q40 1 2Q40 1 2Q40 1 3Q40 1
 1Q40
 1 2Q40 1 1Q40 26R3
 nmattp=10
 1600R3
 nmattp=11
 1600R3
 nmattp=12
 37R3 3R1 5Q40 36R3 4R1 7Q40 35R3 5R1 3Q40 34R3 6R1 3Q40 33R3 7R1 2Q40
 32R3 8R1
 2Q40 31R3 9R1 1Q40 30R3 10R1 2Q40 29R3 11R1 1Q40 28R3 12R1 27R3 13R1
 1Q40 26R3
 14R1 1Q40

nmattp=13
 15R1 25R3 1Q40 16R1 1Q40 1 1Q40 1 2Q40 1 1Q40 1 1Q40 1 2Q40 1 1Q40 1 1Q40
 1
 1Q40 1 1Q40 1 1Q40 1 1Q40 1 1Q40 1 1Q40 2R1 1Q40 1 1Q40 1 1Q40 2R1
 1Q40
 1 1Q40 1 1Q40 562R1
 nmattp=14
 1040R3 2R1 1Q40 2R1 1Q40 1 1Q40 3R1 1Q40 2R1 1Q40 2R1 1Q40 3R1 1Q40
 3R1 1Q40
 4R1 1Q40 4R1 1Q40 8R1 1Q40 86R1
 nmattp=15
 1078R3 2R1 36R3 4R1 35R3 5R1 33R3 7R1 30R3 10R1 28R3 12R1 25R3 15R1
 22R3 18R1
 18R3 22R1 14R3 26R1 6R3 154R1
 nmattp=16
 25R3 15R1 1Q40 24R3 16R1 23R3 17R1 1Q40 22R3 18R1 21R3 19R1 20R3 20R1
 19R3
 21R1 1Q40 18R3 22R1 17R3 23R1 16R3 24R1 15R3 25R1 14R3 26R1 13R3 27R1
 12R3
 28R1 11R3 29R1 10R3 30R1 8R3 32R1 7R3 33R1 6R3 34R1 5R3 35R1 3R3 37R1
 2R3
 638R1
 / material distribution for zlev= 2
 /
 nmattp=17
 798R1 2R5 37R1 3R5 36R1 4R5 34R1 6R5 33R1 5R5 34R1 5R5 34R1 5R5 34R1
 5R5 34R1
 5R5 5R1 4 28R1 4R5 5R1 3R4 27R1 4R5 5R1 4R4 26R1 4R5 5R1 5R4 25R1 4R5
 5R1 6R4
 24R1 4R5 5R1 7R4 23R1 5R5 4R1 8R4 22R1 5R5 4R1 9R4 22R1 4R5 4R1 10R4
 21R1 4R5
 4R1 11R4 20R1 4R5 4R1 12R4 19R1 4R5 5R1 12R4 19R1 4R5 4R1 13R4
 nmattp=18
 308R1 12R5 23R1 17R5 20R1 20R5 16R1 15R5 23R1 11R5 26R1 10R5 28R1 9R5
 15R1 7R4
 7R1 8R5 12R1 13R4 5R1 7R5 10R1 18R4 3R1 7R5 9R1 20R4 2 1 7R5 8R1 21R4
 3R2 6R5
 8R1 21R4 5R2 5R5 7R1 23R4 5R2 3R5 7R1 24R4 6R2 5 7R1 26R4 6R2 6R1 28R4
 6R2 4R1
 30R4 6R2 3R1 31R4 6R2 1 33R4 6R2 35R4 1Q40 4 1Q40 2R4 1Q40 402R4
 nmattp=13
 15R1 25R3 1Q40 16R1 1Q40 1 1Q40 1 2Q40 1 1Q40 1 1Q40 1 2Q40 1 1Q40 1 1Q40
 1
 1Q40 1 1Q40 1 1Q40 1 1Q40 1 1Q40 1 1Q40 2R1 1Q40 1 1Q40 1 1Q40 2R1
 1Q40 1 1Q40 1 1Q40 562R1

nmattp=14
 1040R3 2R1 1Q40 2R1 1Q40 1 1Q40 3R1 1Q40 2R1 1Q40 2R1 1Q40 3R1 1Q40
 3R1 1Q40
 4R1 1Q40 4R1 1Q40 8R1 1Q40 86R1
 nmattp=15
 1078R3 2R1 36R3 4R1 35R3 5R1 33R3 7R1 30R3 10R1 28R3 12R1 25R3 15R1
 22R3 18R1
 18R3 22R1 14R3 26R1 6R3 154R1
 nmattp=16
 25R3 15R1 1Q40 24R3 16R1 23R3 17R1 1Q40 22R3 18R1 21R3 19R1 20R3 20R1
 19R3
 21R1 1Q40 18R3 22R1 17R3 23R1 16R3 24R1 15R3 25R1 14R3 26R1 13R3 27R1
 12R3
 28R1 11R3 29R1 10R3 30R1 8R3 32R1 7R3 33R1 6R3 34R1 5R3 35R1 3R3 37R1
 2R3
 638R1
 / material distribution for zlev= 2
 /
 nmattp=17
 798R1 2R5 37R1 3R5 36R1 4R5 34R1 6R5 33R1 5R5 34R1 5R5 34R1 5R5 34R1
 5R5 34R1
 5R5 5R1 4 28R1 4R5 5R1 3R4 27R1 4R5 5R1 4R4 26R1 4R5 5R1 5R4 25R1 4R5
 5R1 6R4
 24R1 4R5 5R1 7R4 23R1 5R5 4R1 8R4 22R1 5R5 4R1 9R4 22R1 4R5 4R1 10R4
 21R1 4R5
 4R1 11R4 20R1 4R5 4R1 12R4 19R1 4R5 5R1 12R4 19R1 4R5 4R1 13R4
 nmattp=18
 308R1 12R5 23R1 17R5 20R1 20R5 16R1 15R5 23R1 11R5 26R1 10R5 28R1 9R5
 15R1 7R4
 7R1 8R5 12R1 13R4 5R1 7R5 10R1 18R4 3R1 7R5 9R1 20R4 2 1 7R5 8R1 21R4
 3R2 6R5
 8R1 21R4 5R2 5R5 7R1 23R4 5R2 3R5 7R1 24R4 6R2 5 7R1 26R4 6R2 6R1 28R4
 6R2 4R1
 30R4 6R2 3R1 31R4 6R2 1 33R4 6R2 35R4 1Q40 4 1Q40 2R4 1Q40 402R4
 nmattp=19
 280R1 12R5 1Q40 5R5 1Q40 4R5 28R1 15R5 31R1 11R5 33R1 10R5 11R1 7R4
 15R1 9R5
 9R1 13R4 12R1 8R5 7R1 18R4 10R1 7R5 5R1 2 20R4 9R1 7R5 3R1 3R2 21R4 8R1
 7R5 1
 5R2 21R4 8R1 6R5 5R2 23R4 7R1 5R5 6R2 24R4 7R1 3R5 6R2 26R4 7R1 5 6R2
 28R4 6R1
 6R2 30R4 1Q40 4 1Q40 2R4 1 5R2 35R4 4R2 36R4 2R2 478R4

nmattp=20
 760R1 2R5 1Q40 5 1Q40 5 1Q40 2R5 36R1 5R5 36R1 5R5 36R1 5R5 36R1 5R5
 30R1 4
 6R1 4R5 29R1 3R4 5R1 4R5 28R1 4R4 5R1 4R5 27R1 5R4 5R1 4R5 26R1 6R4 5R1
 4R5
 25R1 7R4 5R1 4R5 24R1 8R4 5R1 4R5 23R1 9R4 4R1 5R5 22R1 10R4 4R1 4R5
 22R1 11R4
 4R1 4R5 21R1 12R4 4R1 4R5 20R1 12R4 5R1 4R5 19R1 13R4 4R1 4R5 19R1
 nmattp=21
 18R1 4R5 4R1 14R4 17R1 4R5 4R1 15R4 17R1 4R5 4R1 12R4 2R1 4 16R1 4R5
 4R1 11R4
 21R1 4R5 3R1 11R4 21R1 4R5 4R1 10R4 22R1 3R5 4R1 11R4 21R1 4R5 4R1 11R4
 21R1
 3R5 4R1 12R4 20R1 4R5 4R1 13R4 19R1 3R5 4R1 14R4 18R1 4R5 4R1 15R4 17R1
 3R5
 4R1 21R4 1Q40 11R1 4R5 3R1 22R4 11R1 3R5 4R1 22R4 10R1 4R5 3R1 23R4
 1Q40 10R1
 3R5 4R1 23R4 10R1 3R5 3R1 24R4 9R1 4R5 3R1 24R4 9R1 3R5 4R1 24R4 9R1
 3R5 3R1
 25R4 8R1 4R5 1Q40 3R1 25R4 8R1 3R5 4R1 1Q40 25R4 8R1 3R5 3R1 26R4 7R1
 4R5 2Q40
 3R1 26R4 7R1 3R5 4R1 1Q40 26R4 7R1 3R5 3R1 27R4 6Q40
 nmattp=22
 120R4 1 1Q40 1 1Q40 1 3Q40 37R4 2R1 38R4 1Q40 1 795R4 4R3 34R4 6R3 33R4
 7R3
 32R4 8R3 31R4 9R3 1Q40 30R4 10R3 3Q40
 nmattp=23
 159R4 1 38R4 2R1 37R4 3R1 3Q40 38R4 2Q40 4 1Q40 681R4 4R3 1Q40 2R3 1Q40
 3 1Q40
 3 1Q40 3 2Q40 3 3Q40 30R4
 nmattp=24
 14R4 4R1 4R5 18R1 15R4 4R1 4R5 17R1 4 2R1 12R4 4R1 4R5 22R1 11R4 4R1
 4R5 22R1
 11R4 3R1 4R5 23R1 10R4 4R1 4R5 22R1 11R4 4R1 1Q40 4R5 21R1 12R4 4R1 3R5
 20R1
 13R4 4R1 4R5 19R1 14R4 4R1 3R5 18R1 15R4 4R1 4R5 12R1 21R4 4R1 1Q40 3R5
 12R1
 22R4 3R1 4R5 11R1 22R4 4R1 3R5 11R1 23R4 3R1 4R5 1Q40 10R1 23R4 4R1 3R5
 10R1
 24R4 3R1 4R5 1Q40 9R1 24R4 4R1 3R5 9R1 25R4 1Q40 3R1 4R5 1Q40 8R1 25R4
 4R1
 1Q40 3R5 8R1 26R4 1Q40 3R1 4R5 2Q40 7R1 26R4 4R1 1Q40 3R5 7R1 27R4
 6Q40 3R1
 3R5 7R1

```

nmattp=25
7R1 3R5 3R1 27R4 6Q40 7R1 3R5 4R1 1Q40 26R4 7R1 4R5 2Q40 3R1 26R4 8R1
1Q40 3R5
4R1 1Q40 25R4 8R1 4R5 1Q40 3R1 25R4 9R1 1Q40 3R5 4R1 24R4 9R1 4R5 1Q40
3R1
24R4 10R1 3R5 4R1 23R4 10R1 4R5 1Q40 3R1 23R4 11R1 3R5 4R1 22R4 11R1
4R5 3R1
22R4 12R1 3R5 4R1 1Q40 21R4 12R1 4R5 4R1 20R4 13R1 1Q40 4R5 4R1 12R4
4R2 3R4
14R1 3R5 4R1 10R4 8R2 4 14R1 4R5 4R1 8R4 10R2 15R1 1Q40 4R5 4R1 6R4
11R2 16R1
4R5 1Q40 4R1 5R4 11R2 17R1 4R5 4R1 1Q40 4R4 11R2 18R1 4R5 4R1 4R4 10R2
nmattp=26
30R4 10R3 3Q40 31R4 2Q40 4 1Q40 4 1Q40 4 1Q40 2R4 1Q40 884R4 2 6Q40 39R4
nmattp=27
412,4 49%

nzonrb=96 0.999 0
methac=1 T
/-----BLOCK V(source)-----
/
rkdef=1.000 T
/
/----- BLOCK VI (BOUNDARY CONDITIONS) -----
/
/ var type Group albedos
ibback=0
ibfrnt=0
jbeast=0
jbwest=0
kbsout=0
kbnort=0 T
/
/----- BLOCK VII (PRINTING CONDITIONS) -----
/
/
nxspr=0 nmatpr=1 ngeopr=1 nsrpr=0 nsumpr=1
meshpr=94I-1 -96
nfdump=1 nsdump=0 njdump=0
nadump=0 T

```

Bibliography

- [1] Phoenix Nuclear Labs, "Neutron Flux Case Studies," [Online]. Available: <http://phoenixnuclearlabs.com/case-study/fast-burst-reactor-replacement/>. [Accessed 5 October 2016].
- [2] G. S. a. A. Haghigat, "PENTRAN Code System Users Guide to Version 9.4X.5 Series," HSW Technologies, Arlington, VA, 2008.
- [3] M. R. Chin, C. A. Manalo and A. Et, "Optimization of Multi-Group Cross Section for Fast Reactor Analysis," *International Conference on Mathematics and Computational Methods*, 2013.
- [4] T. F. Wimett, "Fast Burst Reactors in the USA," Los Alamos Scientific Laboratory, 1965.
- [5] T. I. S. a. G. E. Sjoden, *Memordandum of Agreement between AFIT and the Air Force Technical Applications Center*, Dayton: United States Air Force, 2016.
- [6] W. J. Erwin, "Verification and Validation of MCNP6 for Computing Gamma Radiation Protection Factors," AFIT, Dayton, OH, 2015.
- [7] C. Y. a. A. Haghigat, "PENMSHXP Manual Version 2.7b," Georgia Institute of Technology, Arlington, VA, 2008.
- [8] C. J. Bridgman, *Introduction to the Physics of Nuclear Weapons Effects*, Fort Belvoir, VA: Defense Threat Reduction Agency, 2001.
- [9] J. E.E. Lewis and W.F. Miller, *Computational Methods of Neutron Transport*, La Grange Park, Illinois: American Nuclear Society, 1993.
- [10] G. E. Sjoden, Writer, *PENTRAN-CRT Code Workshop*. [Performance]. Air Force Technical Application Center, 2015.

REPORT DOCUMENTATION PAGE				<i>Form Approved</i> <i>OMB No. 074-0188</i>	
The public reporting burden for this collection of information is estimated to average 1 hour per response, including the time for reviewing instructions, searching existing data sources, gathering and maintaining the data needed, and completing and reviewing the collection of information. Send comments regarding this burden estimate or any other aspect of the collection of information, including suggestions for reducing this burden to Department of Defense, Washington Headquarters Services, Directorate for Information Operations and Reports (0704-0188), 1215 Jefferson Davis Highway, Suite 1204, Arlington, VA 22202-4302. Respondents should be aware that notwithstanding any other provision of law, no person shall be subject to a penalty for failing to comply with a collection of information if it does not display a currently valid OMB control number. PLEASE DO NOT RETURN YOUR FORM TO THE ABOVE ADDRESS.					
1. REPORT DATE (DD-MM-YYYY) 03-23-2017		2. REPORT TYPE Master's Thesis		3. DATES COVERED (From - To) March 2016 - March 2017	
TITLE AND SUBTITLE Modeling the White Sands Missile Range Fast Burst Reactor Using a Discrete Ordinates Code, PENTRAN				5a. CONTRACT NUMBER	
				5b. GRANT NUMBER	
				5c. PROGRAM ELEMENT NUMBER	
6. AUTHOR(S) Schulmeister, Taylor R., First Lieutenant, USAF				5d. PROJECT NUMBER	
				5e. TASK NUMBER	
				5f. WORK UNIT NUMBER	
7. PERFORMING ORGANIZATION NAMES(S) AND ADDRESS(S) Air Force Institute of Technology Graduate School of Engineering and Management (AFIT/ENP) 2950 Hobson Way, Building 640 WPAFB OH 45433-8865				8. PERFORMING ORGANIZATION REPORT NUMBER AFIT-ENP-MS-17-M-104	
9. SPONSORING/MONITORING AGENCY NAME(S) AND ADDRESS(ES) Air Force Technical Application Center Patrick AFB, FL 32925 321-494-7688 aftac.pa@us.af.mil ATTN: AFTAC Public Affairs				10. SPONSOR/MONITOR'S ACRONYM(S) AFTAC	
				11. SPONSOR/MONITOR'S REPORT NUMBER(S)	
12. DISTRIBUTION/AVAILABILITY STATEMENT DISTRUBTION STATEMENT A. APPROVED FOR PUBLIC RELEASE; DISTRIBUTION UNLIMITED.					
13. SUPPLEMENTARY NOTES This material is declared a work of the U.S. Government and is not subject to copyright protection in the United States.					
14. ABSTRACT The goal of this research was to develop and characterize a deterministic model of a fast burst reactor (FBR) using a discrete ordinates neutral particle transport code, PENTRAN. The White Sands Missile Range FBR design was chosen for this research because this FBR is important to the DoD due to its short duration, high energy neutron flux which is representative of the neutron flux output created by a nuclear weapon. One, two, and three dimensional PENTRAN models of the FBR were developed and neutron transport based eigenvalue calculations were performed. These eigenvalue calculations were conducted using two different set of nuclear cross-section data: the Bugle-96 47-energy group library (intended for a thermal reactor design), and a 10-group version of the Bugle-96 library which captured the fast neutron energy groups and a single thermal group. The PENTRAN neutron transport calculation results were compared to an analogous MCNP Monte Carlo model, using continuous energy neutron cross sections. The least computationally expensive PENTRAN neutron flux calculations which also compared favorably with the MCNP calculations, was a 24 direction S4 P _n -T _n based quadrature with a first order Legendre Polynomial (P1) expansion of the scattering term and the 10-energy group neutron cross-section library.					
15. SUBJECT TERMS Neutron Transport, Criticality, Fast Burst Reactor					
16. SECURITY CLASSIFICATION OF:			17. LIMITATION OF ABSTRACT	18. NUMBER OF PAGES	19a. NAME OF RESPONSIBLE PERSON
a. REPORT	b. ABSTRACT	c. THIS PAGE			19b. TELEPHONE NUMBER (Include area code)
U	U	U	UU	110	Lt Col James Fee Jr., AFIT/ENP (937) 255-6565, ext 4438 (james.fee@afit.edu)

Standard Form 298 (Rev. 8-98)
Prescribed by ANSI Std. Z39-18